JOC The Journal of Organic Chemistry
Article
pubs.acs.org/joc

Aggregation-Induced Fluorescence Behavior of Triphenylamine-Based Schiff Bases: The Combined Effect of Multiple Forces

Mingdi Yang,[†,‡] Dongling Xu,[†] Wengang Xi,[†] Lianke Wang,[†] Jun Zheng,[§] Jing Huang,[‡] Jingyan Zhang,[‡] Hongping Zhou,*[,†] Jieying Wu,[†] and Yupeng Tian[†]

[†]College of Chemistry and Chemical Engineering, Key Laboratory of Functional Inorganic Materials Chemistry of Anhui Province, Anhui University, Hefei 230601, P. R. China

[‡]School of Materials and Chemical Engineering, Anhui Jianzhu University, Hefei 230601, P. R. China

[§]Center of Modern Experimental Technology, Anhui University, Hefei 230039, P. R. China

Supporting Information

ABSTRACT: Eight triphenylamine (TPA)-based Schiff bases that exhibit different aggregation-induced emission (AIE) or aggregation-caused quenching (ACQ) behavior in tetrahydrofuran (THF)/water mixtures have been synthesized and characterized. The photophysical properties in solution, aqueous suspension, film, and the crystalline state along with their relationships were comparatively investigated. The single-crystal structures of **1**−**8** indicate that compact $\pi\cdots\pi$ stacking or excimers induce fluorescence quenching of **1**, **2**, **5**, and **7**. However, the existence of *J* aggregates or multiple intra- and intermolecular interactions restrict the intramolecular vibration and rotation, enabling compounds **3**, **4**, **6**, and **8** to exhibit good AIE character. The size and growth process of particles with different water fractions were studied using scanning electron microscopy, which demonstrated that smaller uniformly dispersed nanoparticles in the THF/water mixtures favor fluorescence emission. The above results suggest that the combined effects of multiple forces caused by structural variation have a great influence on their molecular packing, electronic structure, and aggregation-induced fluorescence properties. In addition, piezofluorochromic experiments verified the potential applications of **4** and **6**.

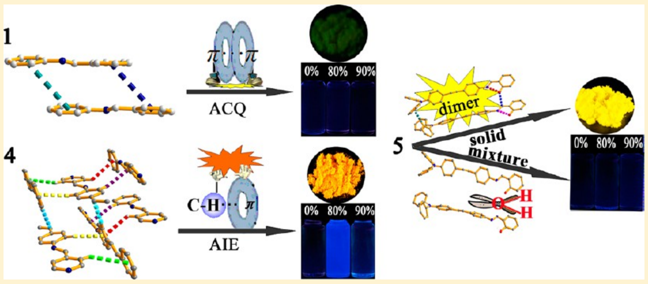

■ INTRODUCTION

π-Conjugated organic materials have attracted much attention because of their potential applications in optoelectronic and photonic applications, such as organic light-emitting diodes (OLEDs),[1−3] cellular imaging,[4,5] detection of microenvironmental changes,[6,7] solar energy conversion,[8−10] organic lasers,[11,12] optical data storage media,[13−15] field-effect transistors (FETs),[16] and so on. Compared with inorganic functional materials, one of the prominent characteristics of organic materials is their structural flexibility. However, most molecules are highly emissive in dilute solutions but become weakly fluorescent or nonemissive when aggregated in poor solvents or fabricated into thin films in the solid state as a result of strong $\pi\cdots\pi$ stacking interactions in extended π-conjugated systems and dipole−dipole interactions.[17−20] This notorious problem of aggregation-caused quenching (ACQ) must be properly tackled because luminophors are commonly used as solid films in their practical applications.

In 2001, the property of aggregation-induced emission (AIE) was observed by Tang and co-workers[21] in silole-based organic molecules, an important class of anti-ACQ materials. 1-Methyl-1,2,3,4,5-pentaphenylsilole molecules were hardly emissive in ethanol or chloroform solutions, but their aggregates or solid states were strongly luminescent. Since then, AIE materials have attracted considerable research attention for their potential application in various fields, such as optoelectronic devices and chemosensors.[22−25] However, the AIE mechanism is difficult to decipher because the AIE effect is against the classical photophysics.[26] The most popular mechanism involves restriction of intramolecular rotation (RIR) in the aggregates.[27,28] Other mechanisms involve restriction of intramolecular charge transfer (ICT),[29] twisted intramolecular charge transfer (TICT),[30,31] and cis−trans isomerization.[32] However, it seems that some of these mechanisms are in conflict, and none of them can be used universally.[33,34] At present there is still much work to do to clarify the AIE behavior from the perspective of the molecular packing and electronic structure.

In this work, we synthesized a new family of triphenylamine (TPA)-based Schiff bases (Scheme 1) that exhibit different AIE or ACQ behavior in THF/water and as solids. Structurally, phenyl, pyridyl, 2-hydroxyphenyl, 4-diethylaminophenyl, 4-diethylamino-2-hydroxyphenyl, and 4-methoxyphenyl groups

Received: August 10, 2013
Published: September 19, 2013

dx.doi.org/10.1021/jo401719c | *J. Org. Chem.* 2013, 78, 10344−10359

Scheme 1. Synthetic Route for Compounds 1−8

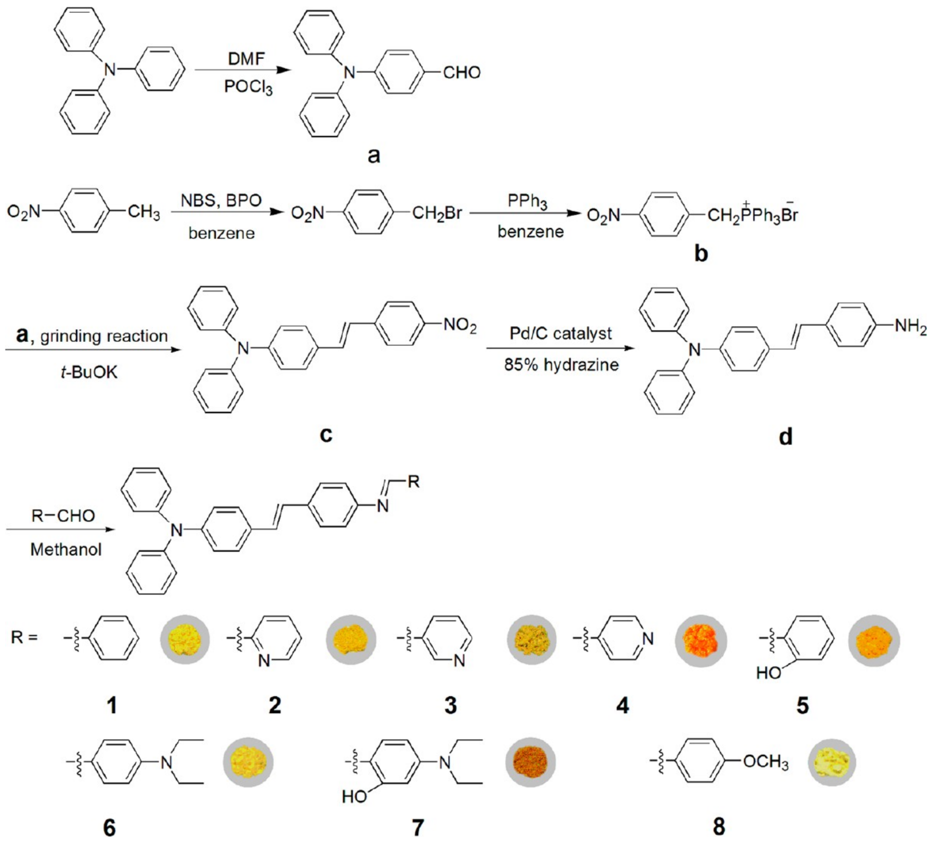

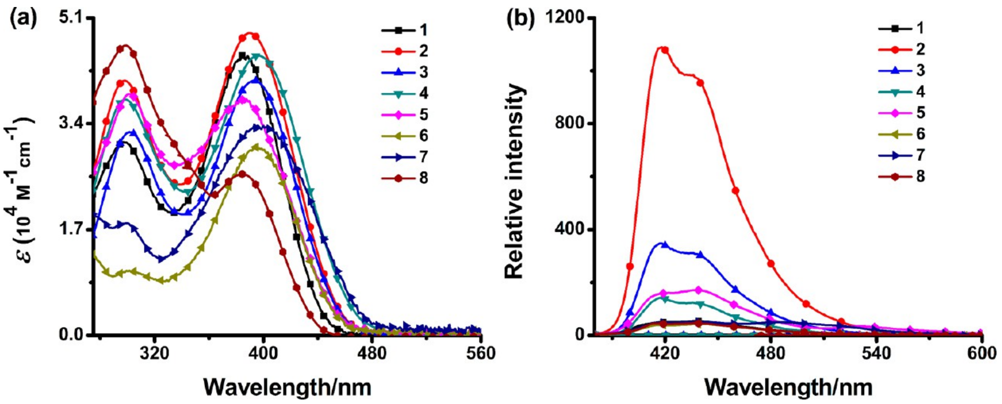

Figure 1. (a) Absorption spectra and (b) PL spectra with excitation wavelength of 385, 390, 393, 396, 384, 395, 394, and 384 nm for **1**−**8**, respectively, in THF with a concentration of 1×10^{-5} mol L^{-1}.

as electron acceptors or donors are intended to enrich the π-electron density and increase the π-electron delocalization of the system. The TPA moiety can not only increase the solubility of the molecule but also enhance the extent of electron delocalization and the ability to donate electrons. Compounds **3**, **4**, **6**, and **8** show good AIE characteristics, but compounds **1**, **2**, **5**, and **7** display ACQ phenomena. The spectroscopic properties of the compounds in solution and in nanosuspensions and their crystal structures were investigated to elucidate the mechanism of enhanced fluorescence in the aggregated state. We aimed to understand how subtle structural changes modulate the AIE or ACQ features of these TPA-based Schiff base, further revealing the structure−property relationship.

■ RESULTS AND DISCUSSION

Design and Synthesis. We designed a series of new luminophors and devised a multistep reaction route for their synthesis (Scheme 1). The intermediate triphenylamine aldehyde 4-(*N*,*N*-diphenylamino)benzaldehyde (**a**), (4-nitrobenzyl)triphenylphosphine bromide (**b**), 4-nitro-4′-(*N*,*N*-diphenylamino)-1,2-stilbene (**c**), and 4-amino-4′-(*N*,*N*-diphenylamino)-1,2-stilbene (**d**) were synthesized efficiently according to the literature.[35,36] Benzaldehyde, 2-pyridinecarboxaldehyde, 3-pyridinecarboxaldehyde, 4-pyridinecarboxaldehyde, salicylaldehyde, 4-diethylaminobenzaldehyde, 4-(diethylamino)salicylaldehyde, and *p*-anisaldehyde were commercially available. Compounds **1**−**8**, respectively, were easily

Table 1. UV–Vis and Fluorescence Data for 1–8 in Dilute THF Solutions, THF/Water Mixtures with Different Water Fractions (f_w), and the Solid State

cmpd		λ_{abs} (nm)[a]	λ_{em} (nm)[b]	τ_1 (ns)[c]	τ_2 (ns)[c]	$\langle\tau\rangle$ (ns)[d]	χ^2	Φ_F[e]
1	solution	298, 385	420	0.50 (84%)	1.47 (16%)	0.66	1.21	<0.1%
	solid	310, 395	515	<0.01				<0.1%
2	solution	298, 390	418	0.44 (99%)	1.35 (1%)	0.46	1.02	4.7%
	solid	315, 406	508	<0.01				<0.1%
3	solution	302, 393	418	0.46 (95%)	1.37 (5%)	0.51	1.27	<0.1%
	f_w = 80%	302, 368	436					15.2%
	f_w = 90%	309, 389	447					<0.1%
	solid	321, 399	523	<0.01				0.1%
4	solution	299, 396	417	0.39 (99%)	2.70 (1%)	0.41	1.12	7.3%
	f_w = 80%	302, 367	432					13.7%
	f_w = 90%	312, 388	417					<0.1%
	solid	319, 399	580	0.58 (56%)	1.95 (44%)	1.18	1.34	8.7%
5	solution	301, 384	422	0.44 (82%)	1.58 (18%)	0.64	1.01	0.4%
	solid	311, 390	555	0.53 (99%)	3.17 (1%)	0.55	1.09	5.2%
6	solution	302, 395	418	0.44 (86%)	1.10 (14%)	0.53	1.28	<0.1%
	f_w = 60%	301, 352	437					8.1%
	f_w = 90%	312, 400	435					<0.1%
7	solid	320, 387	512	<0.01				0.2%
	solution	300, 394	416	0.58 (45%)	1.85 (55%)	1.28	1.14	1.1%
	solid	319, 399	527	<0.01				<0.1%
8	solution	299, 384	415	0.51 (92%)	1.23 (7%)	0.59	1.10	<0.1%
	f_w = 70%	290, 367	437					20.0%
	f_w = 90%	308, 395	420					<0.1%
	solid	314, 387	508	<0.01				0.4%

[a] λ_{abs} = maximal absorption wavelength. [b] λ_{em} = maximal emission wavelength. [c] Fluorescence lifetime and (in parentheses) percent contribution. [d] Weighted mean lifetime. [e] Fluorescence quantum yield as measured using an integrating sphere.

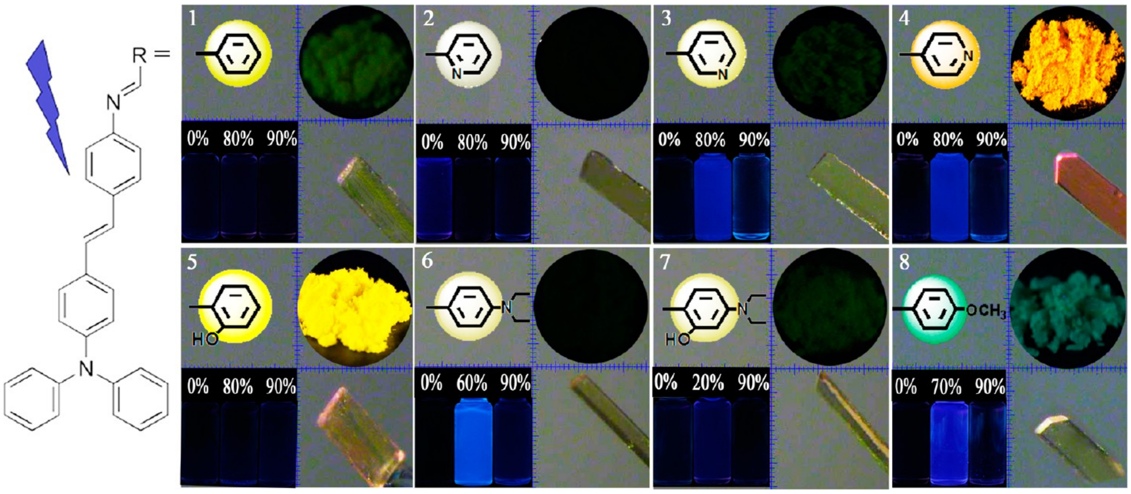

Figure 2. Fluorescent images of **1**–**8** in THF (5×10^{-6} mol L^{-1}), THF/water (20/80 v/v), THF/water (40/60 v/v), THF/water (30/70 v/v), or THF/water (10/90 v/v) or in powder form upon excitation with a 365 nm light source and photographs of the crystals.

synthesized from these aldehydes in high yields via nucleophilic addition reactions with **d**.

All of the intermediates and target compounds were characterized by IR and NMR spectroscopy and mass spectrometry, which confirmed their expected molecular structures. Single crystals of compounds **1**–**8** were obtained by slow evaporation from solutions in dichloromethane (DCM)/acetonitrile or DCM/ethyl acetate mixtures at room temperature and further characterized crystallographically. Their ORTEP drawings are shown in Figures 7a–14a, and Table 2 summarizes the crystal data. All of the luminophors are soluble in common organic solvents, such as acetonitrile, THF, acetone, DCM, *N*,*N*-dimethylformamide (DMF), and chloroform, but have poor solubility in water.

Photophysical Properties. The UV–vis absorption and photoluminescence (PL) emission spectra of the eight compounds in THF solution at a concentration of $c = 1 \times 10^{-5}$ mol L^{-1} are shown in Figure 1. As the molecules have similar structures, the UV–vis spectra are nearly the same. As depicted in Figure 1a, one can see that the absorption spectra exhibit two peaks between 250 and 700 nm, where the low-energy band originates from an ICT process while the high-energy band can be ascribed to the n–π^* transition of the triarylamine moiety (Figures 1 and 15).[37,38] As for the

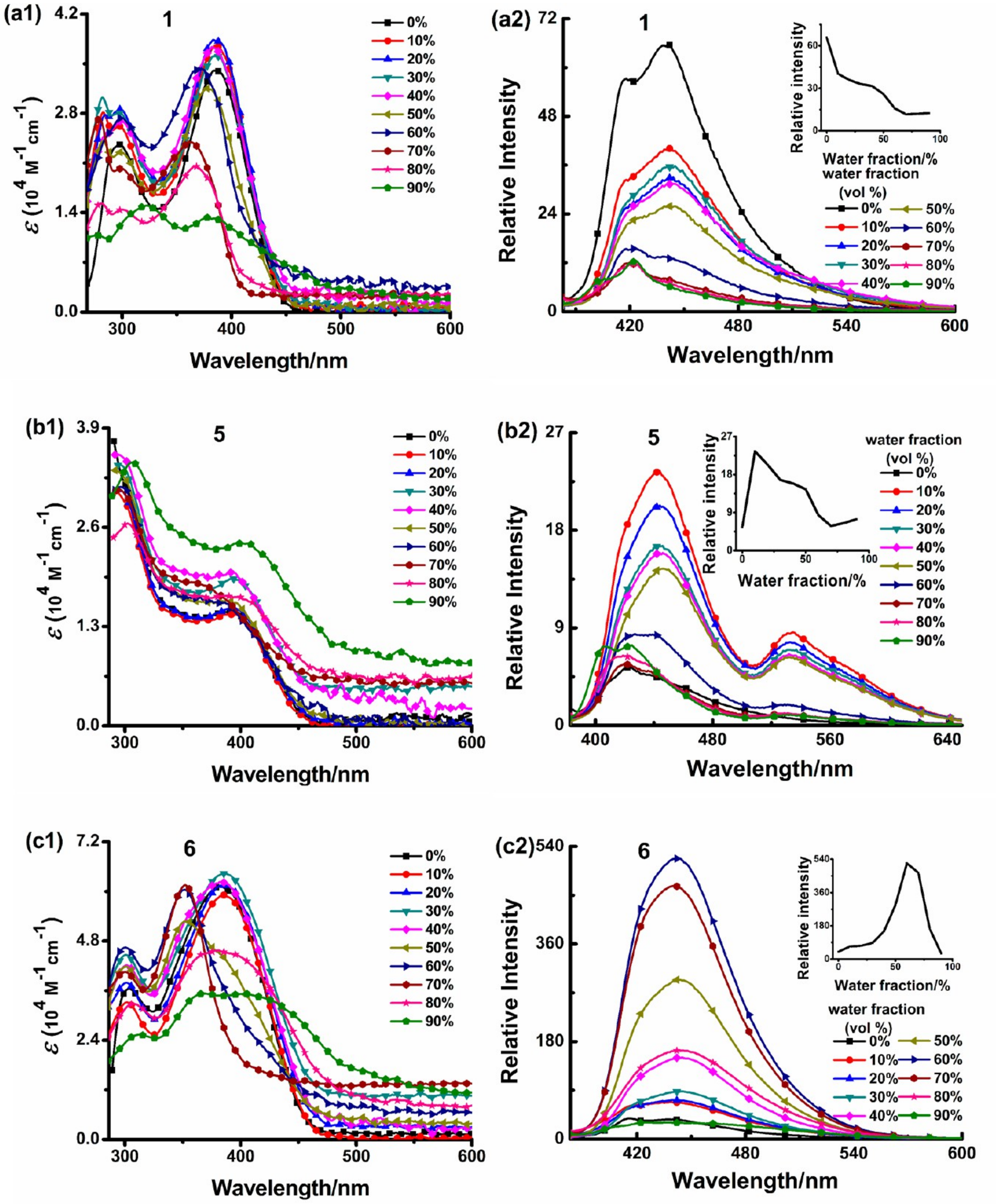

Figure 3. (a1−c1) Absorption and (a2−c2) PL spectra of **1**, **5**, and **6** in THF/water mixtures with different water fractions (f_w). The insets in (a2−c2) depict the changes in the PL peak intensity with different water fractions.

fluorescence emission (Figure 1b), the fluorescence spectra of all eight compounds display two distinct emissions, mainly at ∼418 and ∼430 nm. The former emission is attributed to the emission of the local excited state, whereas the latter is likely assigned to a TICT emission.[31] The THF solutions of **1**−**8** are almost nonluminescent or only weakly luminescent with blue light. The fluorescence quantum yields (Φ_F) of the eight compounds are <0.1, 1.2, 2.2, 1.4, 0.4, <0.1, 1.1, and <0.1%, respectively, in dilute THF solutions (Table 1), as measured using an integrating sphere. It is confirmed that the different substituents have an influence on the electronic structure, producing different optical properties.

Aggregation-Induced Emission. As shown in Figure 2, changing the terminal substituent can lead to different optical properties. Under illumination with a 365 nm UV lamp, only compound **2** displays a weak blue light in pure THF solution, while the other compounds are barely emissive. In the solid state, compounds **1**, **3**, **6**, and **7** emit weak yellow light, **2** is totally nonluminescent, **8** emits cyan light, and **4** and **5** emit bright orange and yellow light, respectively.

To further detect the optical behavior of the aggregation process of these eight compounds, we added different amount of water, a poor solvent for the luminophors, to the pure THF solutions to obtain water fractions (f_w) of 0−90% and then monitored the absorption and PL changes. The concentration was maintained at 5×10^{-6} mol L^{-1}.

Figure 3c2 shows that the PL intensity of **6** changes in aqueous mixtures. In dilute THF solution, **6** is nearly nonemissive, with Φ_F < 0.1%. With gradual addition of water to the THF, the PL intensity of **6** gradually intensifies. From the pure THF solution to THF/water mixture with f_w = 60%, the PL intensity increases by 13.6-fold. At f_w = 60%, a

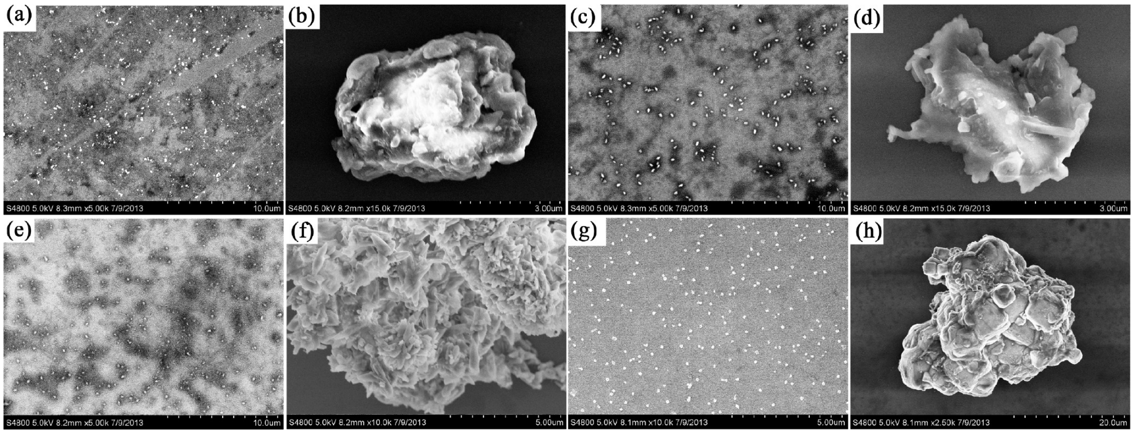

Figure 4. SEM images of **3**, **4**, **6**, and **8** in THF/water mixtures at concentrations of 3×10^{-6} mol L^{-1} with different water fractions: (a) **3** in THF/water (20/80 v/v); (c) **4** in THF/water (20/80 v/v); (e) **6** in THF/water (40/60 v/v); (g) **8** in THF/water (30/70 v/v); (b, d, f, h) **3**, **4**, **6**, and **8**, respectively, in THF/water (10/90 v/v).

maximum Φ_F of 8.1% was recorded (Table 1). This increase in PL intensity can be attributed to the AIE effect. Similar enhancement can be observed in the behavior of **8** (Figure S2 in the Supporting Information). The PL intensity of **8** is enhanced 13.8-fold when f_w increases from 0% to 80%, while at the same time the Φ_F value grows from <0.1% to 20.0%. Compounds **3** and **4** display different fluorescent behaviors from those of **6** and **8** in THF/water mixture solutions with different f_w values (Figure S2). With gradual addition of water to the THF, the emissions of **3** and **4** are dramatically weakened when $f_w \leq 20\%$. The light emission is invigorated from $f_w \approx 20$ vol % and reaches its maximum value at 80% water content, which are 3.8-fold and 8.1-fold higher than that in pure THF solution, respectively. Meanwhile, the maximum emission wavelength is gradually red-shifted to ~435 nm when f_w reaches 80 vol %. This is a typical TICT effect arising from the increased solvent polarity, here achieved by increasing the water fraction.[39,40] These observations can be interpreted as follows: when a large amount of nonsolvent ($f_w > 20\%$) exists in the mixture, molecules of **3** or **4** tend to aggregate; inside the aggregates, the encapsulated molecules are located in a nonpolar environment and the TICT process is limited, and thus, the fluorescence is recovered.[41] As can be seen in Figures 3c2 and S2, after reaching a maximum intensity at 60−80% water content for **3**, **4**, **6**, and **8**, the PL intensities and Φ_F values of the four compounds decrease along with increasing water content. The Φ_F values of **3**, **4**, **6**, and **8** drop from maximum in the THF/water mixture to <0.1% at $f_w = 90\%$. One possible reason for this is that after the aggregation, only the molecules on the surface of the nanoparticles emit light and contribute to the fluorescence intensity upon excitation, which leads to a decrease in fluorescence intensity, but the RIR of the aromatic rings around the carbon−carbon single bonds in the aggregation state enhances the light emission. The net outcome of these two antagonistic processes results in the AIE effect when the water fraction is not higher than 60%, 70%, or 80%. This indicates that the RIR process plays a predominant role in affecting the fluorescent behavior of the aggregated molecules. Furthermore, when the water fraction is higher than 60%, 70%, or 80%, the solubility of these four compounds in the solvent mixture even decreases to yield more insoluble particles, and thus, the number of emitting molecules becomes even less.[42,43] However, there is another possible interpretation. On the one hand, in the mixture with a "low" water content of 60%, 70%, or 80%, molecules of compounds **3**, **4**, **6**, and **8** may steadily cluster together to form ordered, nanoscale aggregates. On the other hand, in the mixture with a very high water fraction of 90%, the compound molecules may abruptly agglomerate to form random, amorphous aggregates. The former leads to an enhancement in the PL intensity, while the latter leads to a reduction in intensity. However, it is hard to control the formation of nanoparticles at high water content. Thus, the measured PL intensity often shows no regularity at high water content.[44,45] Different from **3**, **4**, **6**, and **8**, with the addition of water the emissions of **5** and **7** turn up sharply from 0 to 10% or 30%, respectively. This phenomenon may occur because the intramolecular hydrogen bond formed between the imine and *o*-hydroxyl groups of these compounds may be disrupted when a little bit of water is added to the THF, which can lead to increased PL intensity. After reaching the maximum, the PL intensity declines gradually (Figures 3b2 and S2). There are mainly a dual peak at 400−450 nm and a broad peak around 500−550 nm. Therefore, solutions of compounds **5** and **7** display a typical excimer-related fluorescence character. The former dual peak is assigned to the monomer emission, and the latter broad one could be related to the excimer emission.[46] As shown in Figures 3a2 and S2, with an increase in the water fraction, the PL spectra of compounds **1** and **2** show a descending tendency. For compounds **1**−**8**, the changes of the integrals under the emission bands with different water fractions (f_w) were analyzed and found to be in line with the changes in PL peak intensity with corresponding water fraction (Figure S4 in the Supporting Information).

The absorption spectra of **1**−**8** in aqueous mixtures are shown in Figure 3 and Figure S2 in the Supporting Information. The spectral profiles of **1**−**8** are significantly changed when $f_w > 50$−70%. Meanwhile, the absorption peak at 390 nm with a shoulder around 470 nm emerges initially, which implies that the compound molecules have aggregated into nanoparticles in the aqueous mixtures, because it is well-known that the Mie effect of the nanoparticles causes such leveling-off tails in the absorption spectra.[47,48] In order to determine whether these compounds can form nanostructures, the growth progresses of **3**, **4**, **6**, and **8** were studied by scanning electron microscopy (SEM) with different water fractions (Figure 4).

For **3** (Figure 4a,b and Figure S5 in the Supporting Information), upon injection of THF into the mixture of

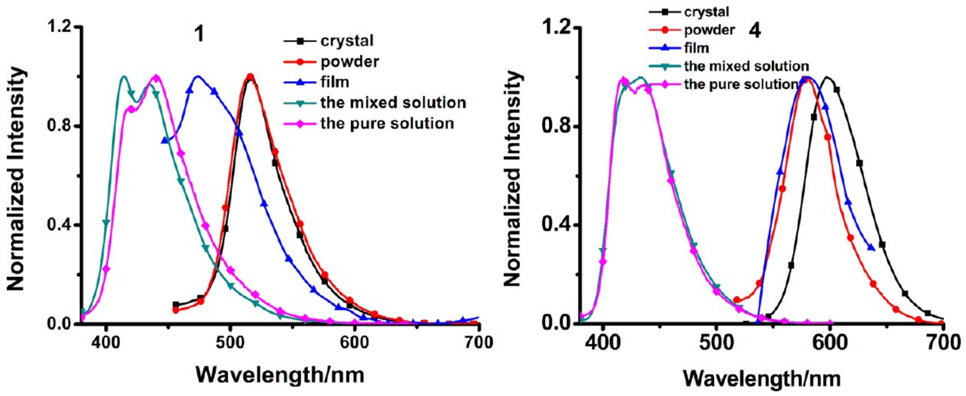

Figure 5. PL spectra of **1** and **4** in the pure solvent, the mixed solvent with f_w = 80%, the film, the powder, and the crystal.

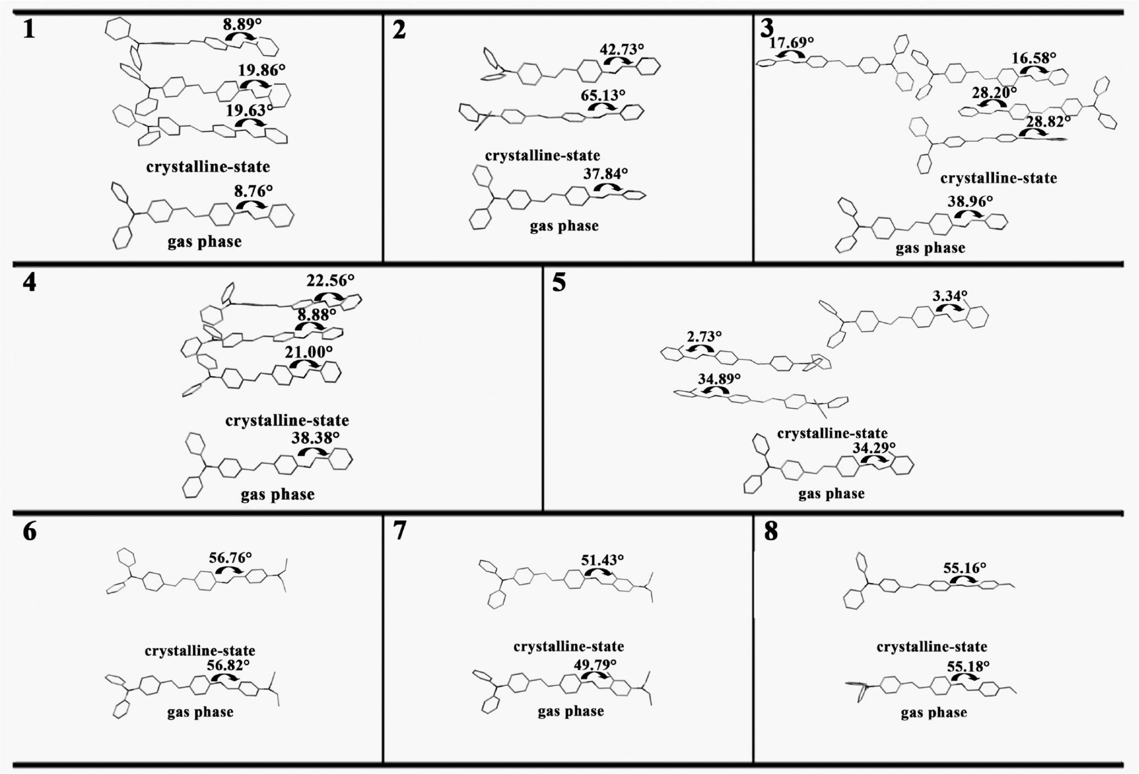

Figure 6. Molecular structures of **1**−**8** in the crystal and in the gas phase.

THF/water (20/80 v/v), nanoparticles emerged immediately with a size range of 80−400 nm. In the mixture of THF/water (10/90 v/v), most of the **3** molecules aggregated together rapidly to form larger amorphous particles. For **4**, **6**, and **8** (Figure 4c,e,g), the nanoparticles were separately dispersed, and the sizes of the nanoparticles reached 70−350, 50−350, and 60−250 nm in the THF/water mixtures (40/60−20/80 v/v), respectively. When f_w reached 90 vol %, the SEM and transmission electron microscopy (TEM) images and electron diffraction (ED) patterns indicated that the aggregates formed in the mixtures were amorphous-like aggregates (Figures 4d,f,h and S5). These phenomena suggest that the observed changes in PL intensity are correlated with the THF/water ratio.[49,50] The formation of nanoparticles is advantageous for fluorescence emission, while the formation of amorphous particles can lead to a reduction in PL intensity.

To make a quantitative comparison, we measured Φ_F for the molecules in the crystal state. The experimental errors from sample concentrations and instruments are estimated to be ±12%. The Φ_F values of solid **3**, **4**, **6**, and **8** are 0.1%, 8.7%, 0.2%, and 0.4%, respectively, which are higher than those of **3**, **4**, **6**, and **8** in solution (Φ_F < 0.1% for **3**, **6**, and **8** and Φ_F = 7.3% for **4**) and manifest their AIE feature (Table 1). On the contrary, the Φ_F values of solid **1**, **2**, and **7** are <0.1%, which are equal to or much lower than those of their THF solutions (Φ_F < 0.1% for **1** and **2** and Φ_F = 1.1% for **7**). In contrast, the Φ_F value of **5** in the solid state is higher than that of its THF solution (Φ_F = 5.2% for the solid and Φ_F = 0.4% for the solution), which is associated with the formation of excimers. Apparently, the changes in Φ_F in going from solution to the crystal also are consistent with the opposite aggregation-induced fluorescence behaviors of **1**−**8** (Table 1), which may be caused by the difference of the substitution group.

The PL decay dynamics of the compounds **1**−**8** were studied by a time-resolved technique (Table 1 and Figure S3 in the Supporting Information). The experimental errors from sample

Table 2. Crystallographic Data for **1**−**8**

	1	**2**	**3**	**4**	**5**	**6**	**7**	**8**
empirical formula	$C_{33}H_{26}N_2$	$C_{32}H_{25}N_3$	$C_{32}H_{25}N_3$	$C_{32}H_{25}N_3$	$C_{99}H_{78}N_6O_3$	$C_{37}H_{35}N_3$	$C_{37}H_{35}N_3O$	$C_{34}H_{28}N_2O$
formula weight	340.42	451.55	451.55	451.55	1399.67	521.68	537.68	480.58
crystal system	triclinic	monoclinic	monoclinic	triclinic	triclinic	triclinic	triclinic	monoclinic
space group	$P\bar{1}$	$P2_1/c$	$P1$	$P\bar{1}$	$P\bar{1}$	$P\bar{1}$	$P\bar{1}$	$P2_1/c$
a (Å)	9.806(3)	10.872(10)	9.488(5)	9.7586(12)	10.453	9.289(5)	9.2815(10)	24.174(5)
b (Å)	15.377(5)	38.16(4)	9.065(5)	15.4226(19)	15.215	9.450(5)	9.4972(10)	9.8145(19)
c (Å)	24.836(8)	11.993(11)	29.064(5)	24.439(3)	24.840	17.389(5)	17.4636(19)	11.092(2)
α (deg)	88.030(4)	90	90	88.839(2)	98.78	83.091(5)	83.778(10)	90
β (deg)	88.733(4)	103.084(14)	98.599(5)	89.370(2)	97.42	89.713(5)	89.848(2)	99.977(5)
γ (deg)	82.218(4)	90	90	82.413(2)	95.99	17.389(5)	74.469	90
V (Å^3)	3708(2)	4846(8)	2471.7(19)	3645.1(8)	3840.5	1460.3(12)	1473.9(3)	2591.9(9)
Z	6	8	4	6	2	2	2	4
T (K)	296(2)	291(2)	298(2)	291(2)	298(2)	298(2)	291(2)	291(2)
D_{calcd} (g cm^{-3})	1.211	1.238	1.213	1.234	1.210	1.186	1.212	1.232
μ (mm^{-1})	0.070	0.073	0.072	0.073	0.073	0.069	0.073	0.074
θ range (deg)	1.55−25.00	1.07−25.00	0.71−24.99	0.83−26.06	0.84−25.03	1.18−25.00	1.17−25.01	0.86−25.10
total no. of reflns	26377	33739	17670	28016	27707	10428	10568	18166
no. of unique reflns	12865	8526	13560	13942	13430	5090	5131	4616
no. of params refined	946	632	1261	947	961	363	373	335
R_1	0.0769	0.0521	0.0517	0.0535	0.1109	0.0447	0.0508	0.0691
wR_2	0.1007	0.0935	0.1368	0.1265	0.2977	0.1429	0.1353	0.2151
GOF	0.976	1.006	1.081	0.930	1.485	1.146	1.049	0.950

concentrations and instruments are estimated to be ±13%. The fluorescence decay behaviors of **1**−**8** in pure THF are well-fitted by a double-exponential function, and the weighted mean lifetimes are 0.66, 0.46, 0.51, 0.41, 0.64, 0.53, 1.28, and 0.59 ns, respectively. Moreover, the solids of **4** and **5** decay through two main relaxation pathways that show obviously longer weighted mean lifetimes than the solutions in pure solvent. The longer lifetimes indicate the existence of new aggregation species or excitonic couplings. The decays of the powders of **1**, **2**, and **7** are too fast to be measured with our equipment (the limit is 0.01 ns).

Additionally, comparison between calculated and experimentally measured fluorescence lifetimes can give additional information and validate the experimental time-resolved technique. The natural radiative lifetime τ_0 and the fluorescence lifetime τ are related through the quantum yield Φ by the equation

$$\Phi = \frac{\tau}{\tau_0} \tag{1}$$

Thus, the fluorescence lifetime of **2** in solution was calculated by multiplying the corresponding quantum yield by the natural lifetime, which could be easily calculated from the known Strickler−Berg equation (eq 2):[51]

$$\frac{1}{\tau_0} = 2.88 \times 10^{-9} n^2 \frac{\int I(\tilde{\nu})\,\mathrm{d}\tilde{\nu}}{\int I(\tilde{\nu})\tilde{\nu}^{-3}\,\mathrm{d}\tilde{\nu}} \int \frac{\varepsilon(\tilde{\nu})}{\tilde{\nu}}\,\mathrm{d}\tilde{\nu} \tag{2}$$

Table 3. Selected Dihedral Angles and Interaction Patterns in the Crystals of 1−8

		dihedral angle (deg)	interaction	*d* (Å)	interaction	*d* (Å)
1	$P_{A1}-P_{A2}$	8.89	C−H···π	2.950	C−H···π	3.407
	$P_{B1}-P_{B2}$	19.86	C−H···π	3.091	C−H···π	2.826
	$P_{C1}-P_{C2}$	19.63	π···π	3.257	π···π	3.687
2	$P_{A1}-P_{A2}$	65.13	C−H···π	3.515	C−H···π	3.672
	$P_{B1}-P_{B2}$	42.73	C−H···π	2.789	π···π	3.130
			π···π	3.313		
3	$P_{A1}-P_{A2}$	16.58	C−H···π	3.232	C−H···π	3.029
	$P_{B1}-P_{B2}$	17.69	C−H···π	3.634	C−H···π	3.200
	$P_{C1}-P_{C2}$	28.82	C−H···π	3.014	C−H···π	3.225
	$P_{D1}-P_{D2}$	28.20	C−H···N	2.707		
4	$P_{A1}-P_{A2}$	21.00	C−H···π	3.144	C−H···π	3.432
	$P_{B1}-P_{B2}$	8.88	C−H···π	3.339	C−H···π	2.849
	$P_{C1}-P_{C2}$	22.56	C−H···π	3.637		
5	$P_{A1}-P_{A2}$	3.34	C−H···π	2.957	N···O	2.587
	$P_{B1}-P_{B2}$	2.73	C−H···π	3.054	N···O	2.601
	$P_{C1}-P_{C2}$	34.89	C−H···π	3.549	N···O	2.618
			C···O	3.103		
6	P_1-P_2	56.76	C−H···π	3.403	C−H···π	2.827
			C−H···π	3.368		
7	P_1-P_2	51.43	C−H···π	2.950	C−H···O	2.651
			N···O	2.597	C−H···O	2.654
8	P_1-P_2	55.16	C−H···π	3.176	C−H···π	3.552
			C−H···π	3.211		

in which n is the refractive index, I is the fluorescence emission, ε is the extinction coefficient, and $\tilde{\nu}$ is the wavenumber. The calculated value of the fluorescence lifetime (0.51 ns) is well-consistent with the experimental value (0.46 ns), thus further validating the experimental time-resolved technique. The calculated values for other compounds are almost all the same as the experimental results.

The Different Properties at the Different States. To further confirm the AIE attribution, we measured a series of PL spectra in solutions with pure solvent, solutions in mixed solvent, films, powders, and single crystals. The crystalline-state geometries were obtained directly from single-crystal data. The gas-phase geometries of **1**−**8** (generally, the molecular geometry in dilute solution can be represented by that of the gas phase) were obtained by geometry optimization in vacuum using their crystallographic data for quantum-chemical modeling.

The PL spectra (Figure 5 and Figure S5 in the Supporting Information) show that **1**−**8** all exhibit their minimum values of λ_{em} in the pure THF and mixed-solvent solutions, their middle values as films and powders, and their maximum values in the form of crystals. The maximum values of λ_{em} in the crystal particles are obviously red-shifted by 99, 85, 106, 181, 139, 137, 90, and 97 nm, respectively, with respect to the values of **1**−**8** in THF solution. Figure 6 shows that the optimized geometries of **3**−**6** and **8** in the gas phase have a twisted conformation with larger torsion angles between the benzene ring and the terminal aromatic ring (38.96°, 38.38°, 34.29°, 56.82°, and 55.18°, respectively) than in the crystalline state (16.58°, 17.69°, 28.20°, and 28.82°; 8.88°, 21.00°, and 22.56°; 2.73°, 3.34°, and 34.89°; 56.76°; and 55.16°, respectively). The distorted conformation destroys the planarity and conjugation of the whole molecule, thus boosting the energy level of the excited state. As a result, blue-shifted emission was observed. Accordingly, effective conjugation in the crystal particles should be favorable for red-shifted emission. Compounds **1**, **2**, and **7** show greater distortion in the crystal state (8.89°, 19.86°, and 19.63°; 42.73° and 65.13°; and 51.43°, respectively) than in the gas phase (8.76°, 37.84°, and 49.79°, respectively), but they display blue-shifted emission in THF solution. These results cannot be explained by the above viewpoint. Therefore, the significantly red-shifted emission in crystalline state compared with the emission in solution must be due to other reasons. To elucidate these phenomena, we prepared and analyzed the single-crystal structures (see below).

Moreover, the redder emission in the powder state suggests that they still suffer from the ACQ problem because of the irregular arrangement in the powder structure.[52] In the solid thin film, the TPA-based derivatives may take relatively twisted but rigid geometries in congested circumstances and thus emit more intensely at shorter wavelengths. Finally, in the mixed-solvent solutions, the molecules may abruptly aggregate into crystal particles. Without the solid constraint, the molecules in the crystal phase may assume a twisted conformation and thus show a redder emission than in the pure THF solution.

Mechanisms of Emission Enhancement. Crystal structure is most important for us to understand the optoelectronic properties and molecular packing. In order to better understand the mechanism, single crystals of **1**−**8** were obtained by slow evaporation from the solutions in DCM/acetonitrile or DCM/ethyl acetate mixtures at room temperature. Their crystal data are summarized in Table 2. The ORTEP diagrams with the N and O atom numbering schemes and some of the packing interactions in the crystals are depicted in Figures 7−14.

As shown in Table 2, compounds **1** and **4**−**7** crystallize in the triclinic system (space group $P\bar{1}$), **2** and **8** crystallize in the monoclinic system (space group $P2_1/c$), and **3** crystallizes in the monoclinic system (space group $P1$). In addition, there are three asymmetric molecules in the unit cells of **1**, **4**, and **5**; two asymmetric molecules in the unit cell of **2**; and one molecule each in the unit cells of **6**, **7**, and **8**. The dihedral angles between the plane of the terminal aromatic ring (P_1) and the

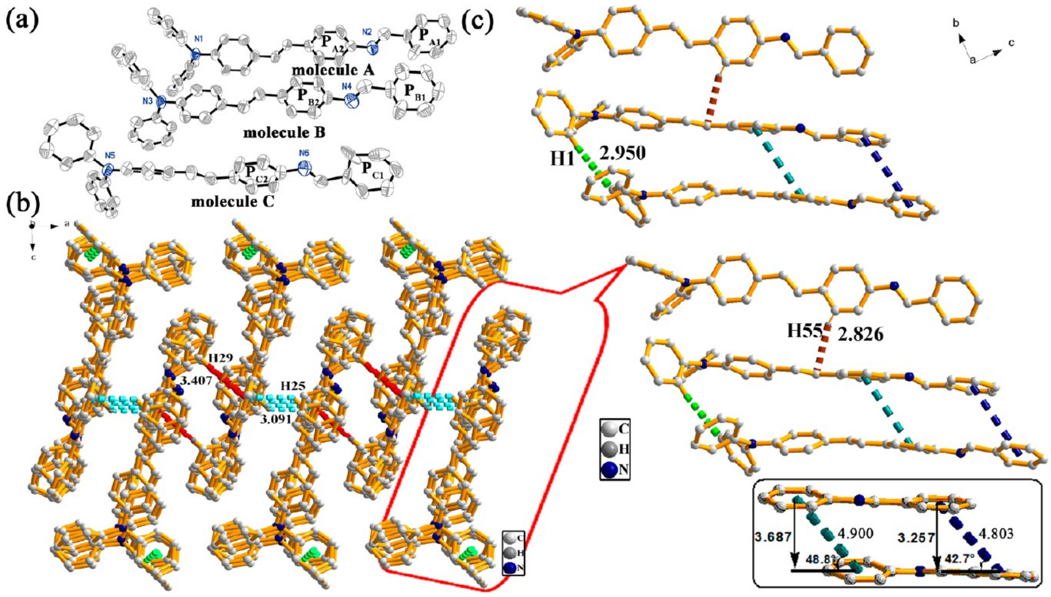

Figure 7. (a) ORTEP diagram of **1**. (b) View of a 1D chain of **1** showing the C−H···π hydrogen bonds (red, light cyan, brown, and green) and π···π stacking (blue and deep green) along the *a* axis. (c) Partial enlarged view of (b). H atoms except H1, H25, H29, and H55 have been omitted for clarity.

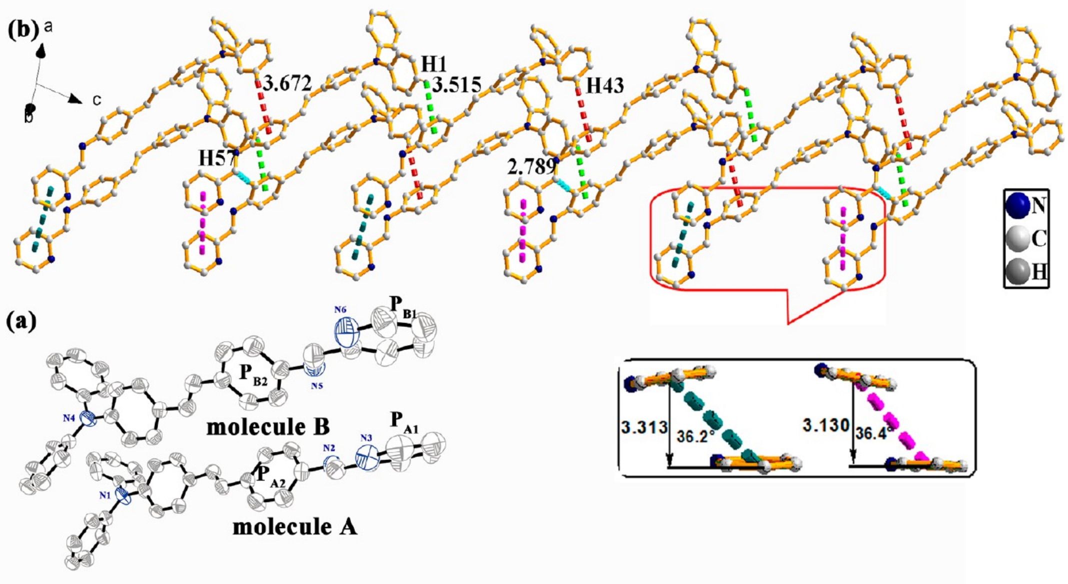

Figure 8. (a) ORTEP diagram of **2**. (b) View of a 1D chain of **2** showing the C−H···π hydrogen bonds (red, light cyan, and green) and π···π stacking (deep green and pink) along the *c* axis. H atoms except H1, H43, and H57 have been omitted for clarity.

plane of the benzene ring (P_2) are 8.89°, 19.86°, and 19.63° for **1**; 65.13° and 42.73° for **2**; 16.58°, 17.69°, 28.82°, and 28.20° for **3**; 21.00°, 8.88°, and 22.56° for **4**; 3.34°, 2.73°, and 34.89° for **5**; 56.76° for **6**; 51.43° for **7**; and 55.16° for **8**. Figures 7−14 show that the molecules of **1**−**8** all have several kinds of weak intra- and intermolecular interactions; the data are given in Table 3. These interactions in the crystals prevent free torsional motions around the double bonds (C═C and C═N), and the molecules are tightly stabilized in the crystal lattice and still have distorted structures resulting from the internal steric hindrance, not only making the molecules more rigid and stable in the crystal lattice but also inducing loose intermolecular packing.

For compound **1**, which possesses only a 1D chain structure, every six molecules are packed into a small unit, and two small units are stacked together to form a repeat unit. Four kinds of C−H···π hydrogen bonds with distances of 2.826, 2.950, 3.091, and 3.407 Å are formed between the hydrogen atoms of the phenyl rings in one molecule and the π cloud of the planar aromatic ring in another molecule (Figure 7b,c). In addition, the distances between the two adjacent molecules A and C are 3.257 Å (P_{A1}−P_{C1}) and 3.687 Å (P_{A2}−P_{C2}) (vertical distances with angles of 42.7° and 48.8°), respectively. The formation of π···π stacking would forbid radiative transition. Therefore, the solid powder or crystal of **1** shows very weak emission.

Compounds **2**−**4** share similar structures of the terminal pyridine ring. As shown in Figure 8, every molecule of **2** is

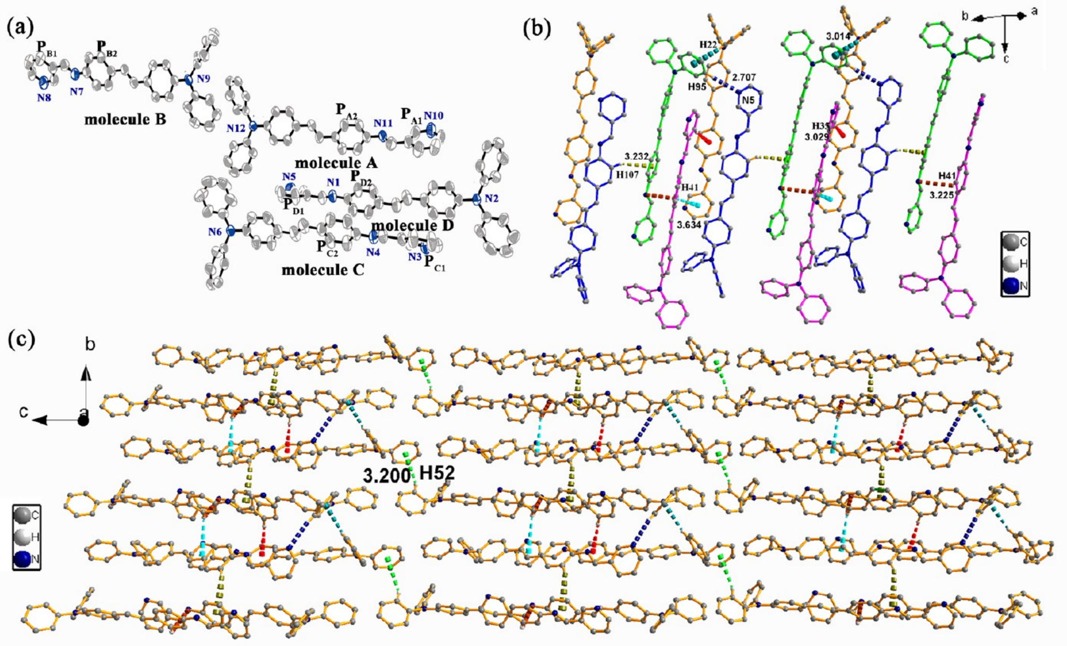

Figure 9. (a) ORTEP diagram of **3**. (b) View of a 1D chain of **3** showing the C−H···π (red, deep green, dark yellow, and light cyan) and C−H···N (blue) hydrogen bonds. (c) View of the 2D layer structure of **3**, showing the C−H···π stacking (green) along the *c* axis. H atoms except H22, H35, H43, H52, and H107 have been omitted for clarity.

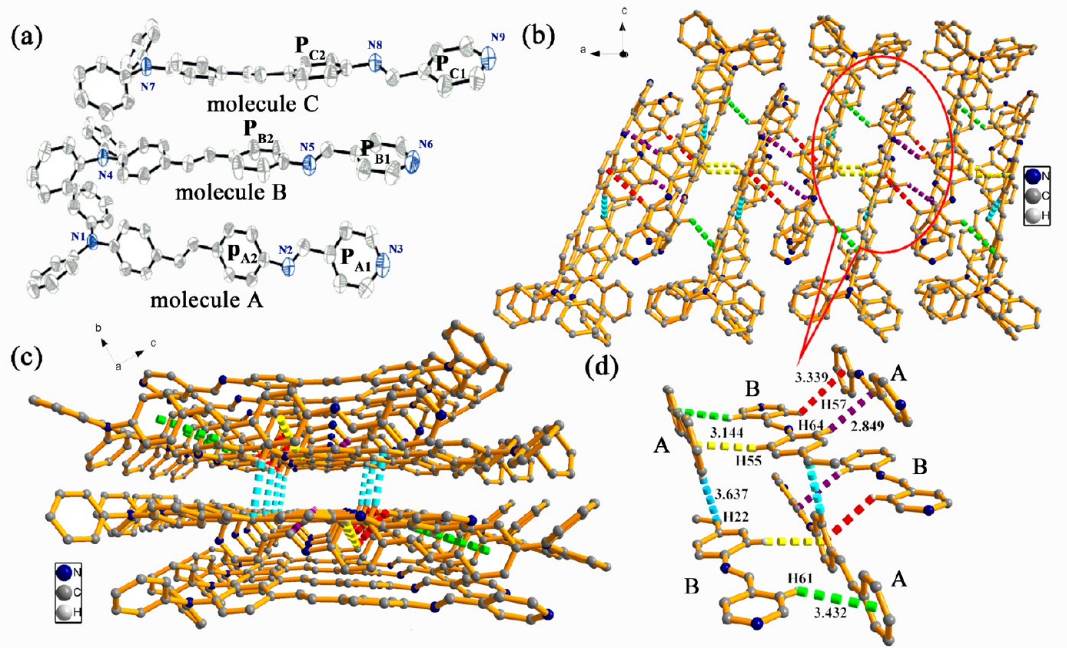

Figure 10. (a) ORTEP diagram of **4**. (b) View of a 1D chain of **4** showing the C−H···π hydrogen bonds (red, green, light cyan, violet, and yellow) viewed along the *b* axis. (c) View of the 1D structure of **4** along the *a* axis. (d) Partial enlarged view of (b). H atoms except H55, H61, and H64 have been omitted for clarity.

packed into an interinserted column structure, and two A molecules and two B molecules are stacked together to form a repeat unit. Furthermore, the 1D chain structure of **2** is formed through three kinds of C−H···π stacking interactions (d = 2.789, 3.515, and 3.672 Å; Figure 8b). However, the distances between the two terminal pyridine rings (P_{A1}−P_{B1}) in a repeat unit are 3.130 and 3.313 Å (vertical distances with angles of 36.4° and 36.2°), respectively, which can weaken the AIE effect and lead to very weak emission or total nonemission of the solid powder and crystal of **2**. However, molecules of **3** are restricted by the C−H···N hydrogen bonds (d = 2.707 Å) and C−H···π stacking interactions (d = 3.014, 3.225, 3.232, and 3.634 Å) (Figure 9), which help to rigidify the molecular conformation and lock the molecular rotation. For **4**, which has only the 1D chain structure Figure 10b,c), each A or B molecule connects adjacent molecules through five kinds of C−H···π stacking interactions (d = 2.849, 3.144, 3.339, 3.432, and 3.637 Å), forming a highly rigid structure. This rigid packing

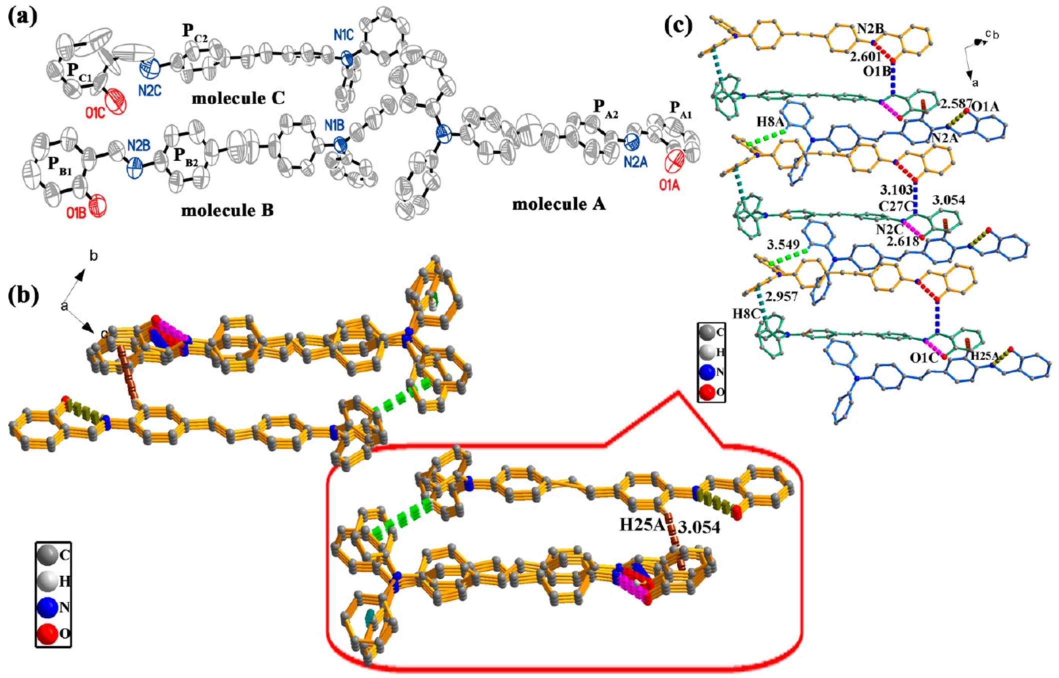

Figure 11. (a) ORTEP diagram of **5**. (b) View of the 1D layer structure of **5** showing the C−H···π hydrogen bonds (deep green, green, and brown), N···O bonds (red, pink, and olive-drab), and C···O bond (blue) along the *a* axis. (c) View of the red-circled section in (b). H atoms except H8A, H8C, and H25A have been omitted for clarity.

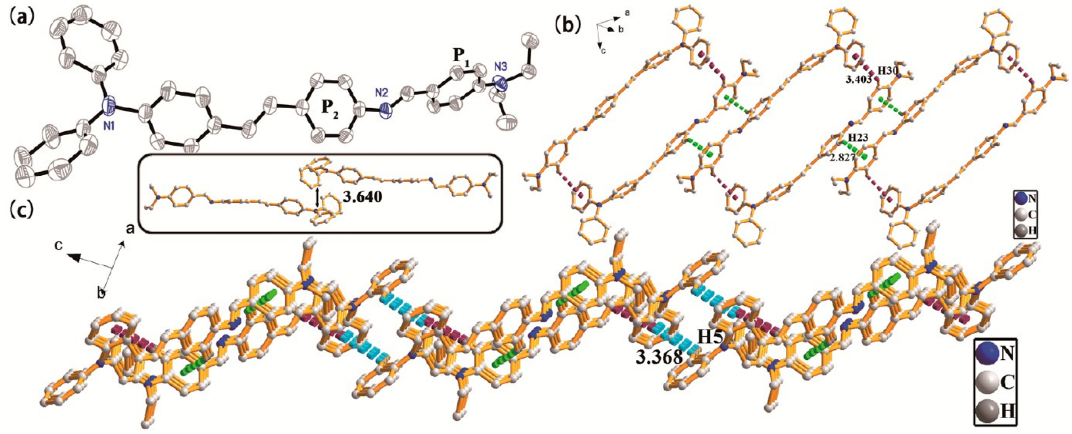

Figure 12. (a) ORTEP diagram of **6**. (b) View of a 1D chain of **6** showing the C−H···π hydrogen bonds (brown and green). (c) View of the 2D chain structure of **6** showing the C−H···π hydrogen bonds (light blue). H atoms except H5, H23, and H30 have been omitted for clarity.

structure can suppress the torsional/vibrational motions of the molecules of **4**, which is helpful for fluorescence emission. The dihedral angle between adjacent molecules A and B is 89.25° ($P_{A2}-P_{B2}$), indicating an almost perpendicular arrangement; thus, there is no π···π stacking, and neither *J* aggregates nor *H* aggregates are observed in the crystal. Moreover, this almost perpendicular structure makes the molecules form a loose packing structure. As a result, the excited-state energy consumed by intramolecular rotation is greatly reduced, which enables the molecules to emit intensely in the solid state.

Compounds **5** and **7** (Figures 11 and 13, respectively) both have an *o*-hydroxyl group on the terminal benzene ring and form multiple N···O interactions (d = 2.587, 2.601, and 2.618 Å for **5** and 2.597 Å for **7**), which confirmed what we speculated. As shown in Figure 11, compound **5** has only the 1D layer structure, and the molecules A and B have a more planar conformation. The oxygen atom of molecule B forms a C···O bond (d = 3.103 Å) with a carbon atom of the adjacent molecule C, which are bonded together by C−H···π hydrogen bond (d = 2.957 Å) and the C···O bond to form a particular dimer. Compound **7** also forms dimers through two C−H···O hydrogen bonds (d = 2.651 Å). However, compounds **5** and **7** display different fluorescence behaviors in the solid state. For compound **5**, when the dimer is excited, it turns into an excimer without arrangement adjustment, and when the excimer decays back to the dimer, there are no repulsive interactions either. Therefore, the nonradiative decay pathways are greatly blocked, and a strongly enhanced excimer emission in the solid state is induced.[53] Nevertheless, in the THF/water mixed solution, compound **5** is hardly emissive. One possibility is that the hydroxyl groups in the dimers form new intermolecular hydrogen bonds with H_2O molecules from the mixed solution,

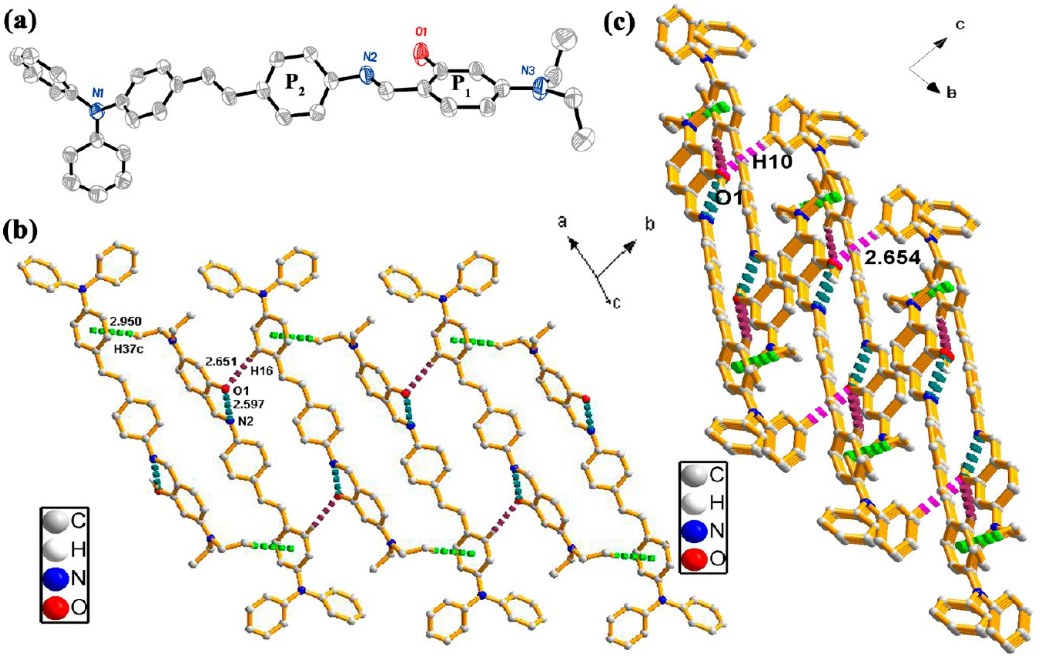

Figure 13. (a) ORTEP diagram of **7**. (b) View of a 1D chain of **7** showing the C−H···π hydrogen bond (green), N···O bond (deep green), and C−H···O hydrogen bond (violet) along the *b* axis. (c) View of the 2D layer structure of **7** showing the C−H···O stacking (pink) along the *a* axis. H atoms except H10, H16, and H37C have been omitted for clarity.

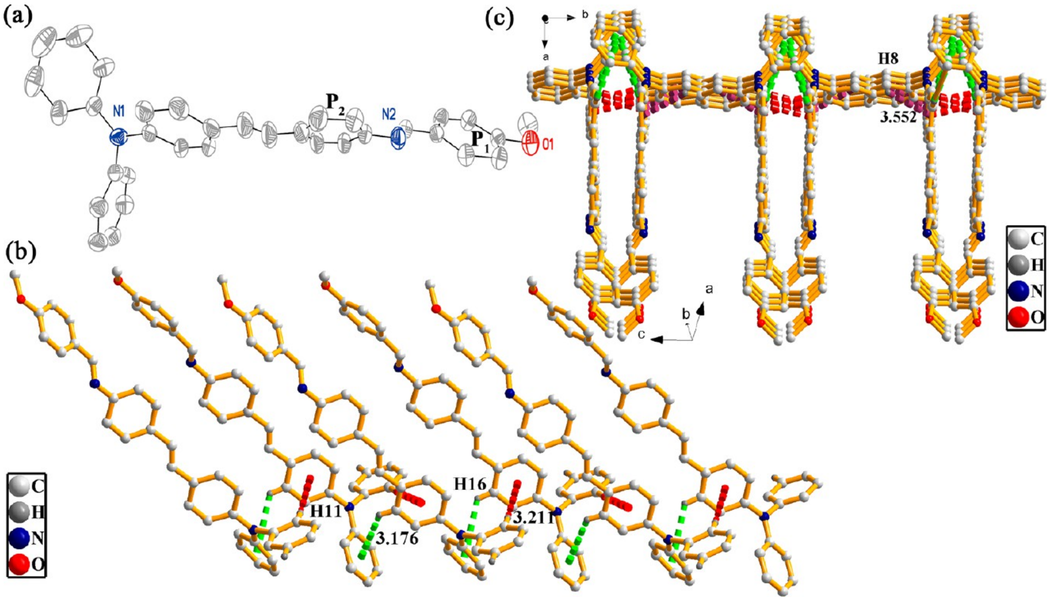

Figure 14. (a) ORTEP diagram of **8**. (b) View of a 1D chain of **8** showing the C−H···π hydrogen bonds (red and green) along the *c* axis. (c) View of the 2D layer structure of **8** showing the C−H···π stacking (violet) along the *b* axis. H atoms except H8, H11, and H16 have been omitted for clarity.

destroying the formation of dimer originally in the crystal, which leads to fluorescence quenching. As far as compound **7** is concerned, the two molecules that form an excimer must first undergo suitable arrangement adjustments to combine together and then a repulsive process to decay to the ground state; these actions consume much excited-state energy and subsequently effectively quench the fluorescence in the solid. In the case of **6**, the molecules are fixed into centrosymmetric antiparallel dimers by the two adjacent molecules. Moreover, both phenyl rings on TPA can form $\pi \cdots \pi$ stacking interactions (a vertical distance of 3.640 Å), resembling that of a *J* aggregation (Figure 12), which can diminish the nonradiative relaxation process and enhance the radiative relaxation process. Three kinds of C−H···π hydrogen bonds are formed between TPA moieties of adjacent molecules in the crystal of compound **8** (Figure 14). This is a common feature of AIE-active molecules.[54−56] These intermolecular interactions help rigidify the conformation and lock the intramolecular rotations of the aromatic ring, inducing loose intermolecular packing, which would be helpful for fluorescence emission.

For compounds **1**−**8**, there are multiple hydrogen bonds such as C−H···π, C−H···N, and C−H···O as well as N···O and C···O bonds and partial $\pi \cdots \pi$ stacking within the single-crystal structure, and these various intermolecular or intramolecular

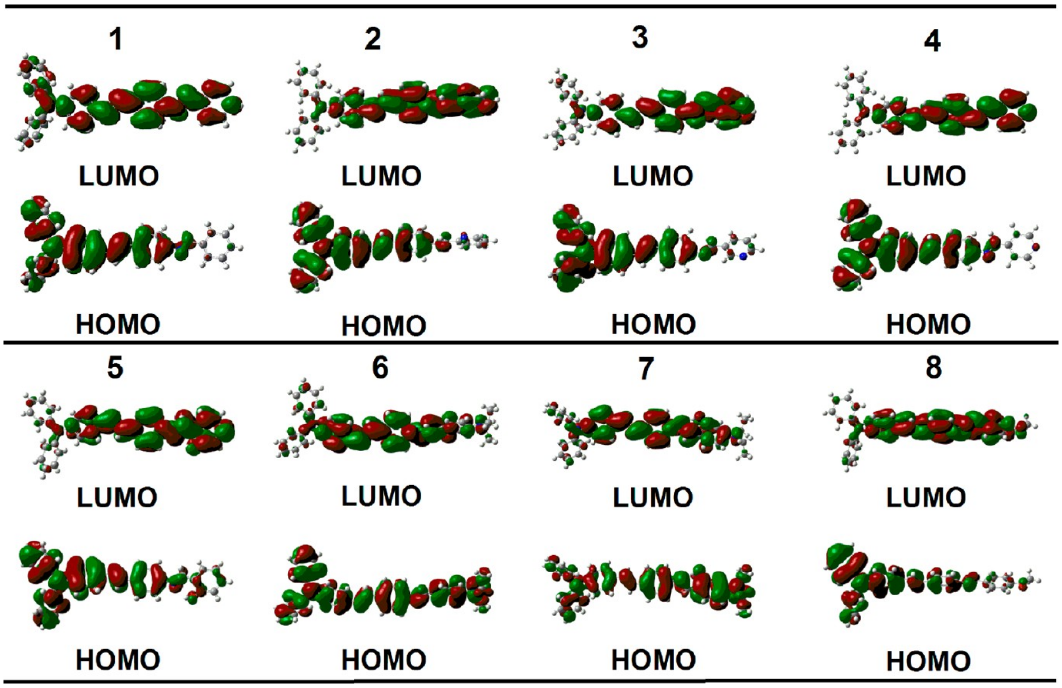

Figure 15. Electron density distributions of the frontier molecular orbitals of compounds **1**−**8**.

interactions help to rigidify the conformation, lock the intramolecular rotations of the aromatic ring and the phenyls against the TPA unit, and enhance the emission. However, these various interactions can have disadvantageous effects on the fluorescence emission as well.[57] Intermolecular interactions also can promote the formation of species such as excimers and exciplexes as well as partial $\pi\cdots\pi$ stacking, which are detrimental to the fluorescence. These two opposite effects compete to determine the aggregation-induced fluorescence behaviors.[58] For the TPA-based Schiff bases, the variations in substitution group bring dramatic changes in the fluorescence spectra. In particular, the intermolecular or intramolecular interaction modes and molecular packing affect the aggregate emission. As for the dual roles of molecular packing in the emission, it is obvious that the advantageous effect outweighs the opposite one for **3**, **4**, **6**, and **8**. Furthermore, the crystal structures of **1**−**8** also indicate that the red-shifted emission in crystalline state compared with the emission in solution depends not only on the planarity of a single molecule but also on the intermolecular forces, such as $\pi\cdots\pi$ stacking and excimers.

Electronic Structure. To understand the relationship between the optical properties and the electronic structure, the HOMOs and LUMOs of **1**−**8** were obtained by DFT/B3LYP/6-31G Gaussian calculations based on the molecule conformations in the crystal structures.[59−61] The optimized geometries and HOMO and LUMO plots are given in Figure 15. All eight molecules adopt twisted conformations whose geometries are similar to the crystal structure of TPA.[54] The results demonstrate that the calculated band gaps of **1**−**8** are different (3.99, 3.32, 3.31, 3.20, 3.95, 3.92, 3.73, and 4.06 eV for **1**−**8**, respectively) and increase in the following order: **4**, **3**, **2**, **7**, **6**, **5**, **1**, and **8**. The results reveal that extension of the π system and electron-withdrawing ability of the acceptor or the electron-donating ability of the donor can both expand the band gaps obviously.

Solid-State Piezochromic Luminescence. We examined the piezofluorochromic (PFC) behaviors of solid **4** and **6** by grinding using a mortar and pestle. The emission spectra of solid **4** and **6** exhibit significant red shifts of 7 nm for **4** and 31 nm for **6** after grinding (Figure 16), denoting that the compound has PFC behavior. The pristine solids **4** and **6** emit orange and yellow fluorescence, respectively. However, when they are ground, **4** is changed into orange-red-emitting under 365 nm UV light, and **6** becomes yellowish-orange-emitting under ambient light (Figure 16). The results suggest that the materials have a color-changeable feature that may possess potential for applications in optical recording and pressure sensing fields.

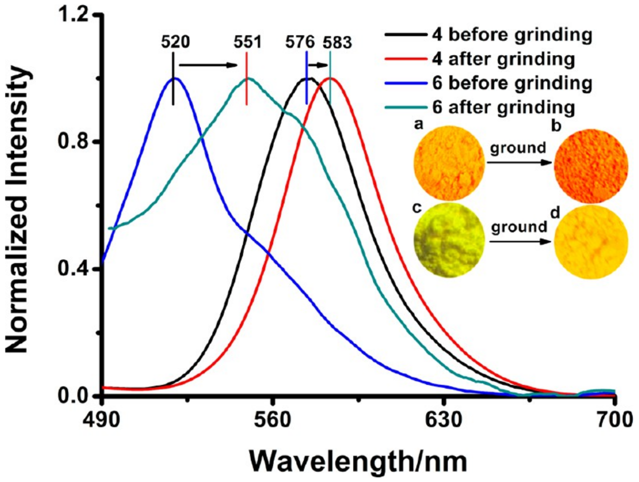

Figure 16. PL spectra and images of **4** and **6** before and after grinding. Images: (a) pristine sample of **4** under UV light; (b) ground sample of **4** under UV light; (c) pristine sample of **6** under ambient light; (d) ground sample of **6** under ambient light.

To identify the mechanism of the PFC behavior, wide-angle X-ray diffraction (WXRD) measurements were performed to gain insight into the mechanical effect on the material.

According to the WXRD measurements (Figure 17), the compound exhibits different structures of molecular aggregation before and after grinding. For compounds **4** and **6** under different conditions, the diffraction curves of the original samples reveal numerous sharp and intense reflections, which indicates crystalline order. The diffraction curves of the samples after grinding show a weak, broad, and diffuse peak, indicating that after grinding the ordered structure has been destroyed and the aggregation structure has become an amorphous state. The result shows that the structural changes in the mode of molecular packing under external grinding can induce a significant PFC property.

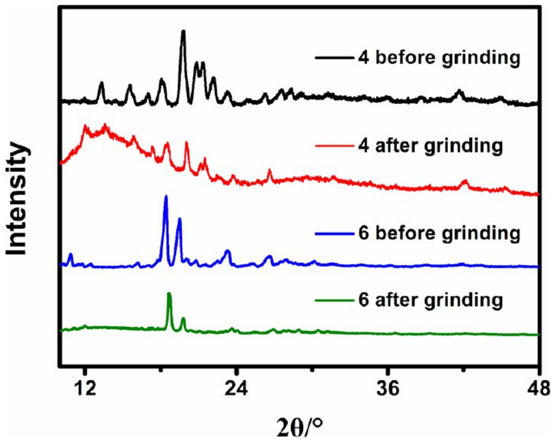

Figure 17. WXRD data for **4** and **6** before and after grinding.

CONCLUSION

In summary, a series of TPA-substituted styrene-based conjugated Schiff bases **1**−**8** with different terminal functional groups have been designed and synthesized. The photophysical properties of compounds **1**−**8** dissolved in THF/H_2O mixtures are remarkably different from those at the molecular level (solution) and in the solid state. SEM images of the compounds in aggregates and single-crystal structures revealed that smaller uniformly dispersed nanoparticles are in favor of fluorescence emissions. The crystallographic data of **1**−**8** state that the formation of excimers and compact $\pi\cdots\pi$ stacking are unfavorable for fluorescence emission, while the formation of *J* aggregates and multiple C−H···π, C−H···N, C−H···O, C···O, and N···O interactions between the adjacent or same molecules restrict the intramolecular rotations and block nonradiative processes, which would induce emissions enhancement. The combined effects of these two opposite factors make compounds **3**, **4**, **6**, and **8** display obvious AIE character, while compounds **1**, **2**, **5**, and **7** exhibit ACQ behavior. DFT calculations yielded HOMOs and LUMOs consistent with the absorption spectra of compounds **1**−**8**. The results demonstrate that the structural variations have a great influence on their photophysical properties, molecular packing, electronic structure, and aggregation-induced fluorescence properties. Furthermore, we have also demonstrated that **4** and **6** can be utilized in optical recording and pressure sensing fields as a result of their excellent structural changes before and after grinding.

EXPERIMENTAL SECTION

General. All of the reagents were obtained commercially and used as purchased. The intermediates **a**, **b**, **c**, and **d** were synthesized efficiently according to the literature.[35,36] IR spectra were recorded with an FT-IR spectrometer (KBr discs) in the 4000−400 cm^{-1} region. NMR spectra were recorded on a 400 MHz NMR instrument using DMSO-d_6 as the solvent. Chemical shifts are reported in parts per million relative to internal TMS (0 ppm), and coupling constants are reported in hertz. Splitting patterns are described as singlet (s), doublet (d), triplet (t), quartet (q), or multiplet (m). Mass spectra were obtained on an LTQ Orbitrap XL mass spectrometer or autoflex-speed MALDI-TOF/TOF mass spectrometer. Melting points were obtained on a Q2000 differential scanning calorimeter at a heating rate of 10 °C/min under a nitrogen atmosphere. SEM images were obtained using a Hitachi S-4800 scanning electron microscope, and TEM images were obtained using a JEM-2010 electron microscope. One-photon absorption spectra were recorded on a UV-265 spectrophotometer. One-photon-excited fluorescence spectra were measured using a Hitachi F-7000 fluorescence spectrophotometer. Single-crystal X-ray diffraction measurements were performed on a Bruker Smart 1000 CCD area detector using graphite-monochromatized Mo Kα radiation (λ = 0.71069 Å). Intensity data were collected in the variable-ω scan mode. The structures were solved by direct methods and difference Fourier syntheses. Non-hydrogen atoms were refined anisotropically, and hydrogen atoms were introduced geometrically. Calculations were performed with the SHELXTL-97 program package. For time-resolved fluorescence measurements, the fluorescence signals were collimated and focused onto the entrance slit of a monochromator with the output plane equipped with a photomultiplier tube. The decays were analyzed by least-squares. The quality of the exponential fits was evaluated by the goodness of fit (χ^2). The absolute photoluminescence quantum yields (Φ_F) of the solid and THF solution (5×10^{-6} mol L^{-1}) were determined using an integrating sphere. Time-resolved fluorescence measurements were performed on a HORIBA FluoroMax-4P fluorescence spectrofluorometer. Powder X-ray diffraction experiments were performed on a Bruker D8 Advance powder X-ray diffractometer with Cu Kα radiation and a LyneEye detector. Crystallographic data (excluding structure factors) for the structure(s) reported in this paper have been deposited with the Cambridge Crystallographic Data Centre as supplementary publications CCDC952622, 932891, 932892, 932893, 945197, 945198, 945199, and 945200.

Preparation of 1. A 2.6 g (7.2 mmol) sample of **d** and 120 mL of methanol were added into a round-bottom flask equipped with a magnetic stirrer and heated at 70 °C for 10 min. A few drops of glacial acetic acid were then added to the preceding reaction system, and 1 g (9.4 mmol) of benzaldehyde was added dropwise. The reaction mixture was refluxed for about 6 h and monitored by TLC. After the completion of the reaction, the reaction mixture was filtered under vacuum immediately to give 2.2 g of a yellow powder. Yield: 67.9%. Mp: 189 °C. ^{1}H NMR (DMSO-d_6, 400 Hz): δ 6.97 (d, *J* = 8.0 Hz, 3H), 7.03−7.07 (m, 6H), 7.19 (d, *J* = 12.0 Hz, 2H), 7.28−7.35 (m, 6H), 7.51−7.53 (m, 5H), 7.63 (d, *J* = 8.0 Hz, 2H), 7.95 (t, *J* = 8.0 Hz, 2H), 8.68 (s, 1H). ^{13}C NMR (100 MHz, DMSO-d_6, TMS): δ 160.0, 151.1, 147.9, 147.8, 136.7, 136.1, 131.9, 131.8, 129.7, 129.2, 128.1, 127.7, 127.5, 126.7, 124.9, 123.8, 123.5, 121.8. IR ν: 3027, 2922, 1589, 1509, 1492, 1277, 1171, 963, 837, 753, 695, 551 cm^{-1}. HRMS (ESI-MS) *m*/*z*: calcd for $[M]^+$, 450.210; found, 449.890.

Preparation of 2. Compound **2** was prepared according to a procedure similar to that for **1**, using 2-pyridinecarboxaldehyde (1 g, 9.35 mmol) instead of benzaldehyde, to give 3.05 g of yellow powder. Yield: 88.4%. Mp: 165 °C. ^{1}H NMR (DMSO-d_6, 400 Hz): δ 7.03−7.06 (m, 6H), 7.10−7.12 (m, 4H), 7.24−7.26 (m, 4H), 7.28−7.32 (m, 3H), 7.39 (d, *J* = 8.0 Hz, 2H), 7.54 (d, *J* = 8.0 Hz, 2H), 7.80 (t, *J* = 6.0 Hz, 1H), 8.21 (d, *J* = 8.0 Hz, 1H), 8.65 (s, 1H), 8.71 (d, *J* = 8.0 Hz, 1H). ^{13}C NMR (100 MHz, DMSO-d_6, TMS): δ 160.0, 149.7, 149.2, 147.7, 147.1, 146.9, 137.0, 136.2, 131.3, 129.6, 129.4, 127.9, 127.6, 127.2, 126.2, 124.1, 123.3, 122.9, 121.8, 121.2. IR ν: 3024, 1585, 1508, 1493, 1327,1288, 968, 833, 752, 694, 553 cm^{-1}. MALDI-TOF m/z: calcd for [M + H]$^+$, 452.205; found, 452.925.

Preparation of 3. Compound **3** was prepared according to a procedure similar to that for **1**, using 3-pyridinecarboxaldehyde (1 g, 9.35 mmol) instead of benzaldehyde, to produce 3.1 g of yellow needle crystals. Yield: 90.0%. Mp: 181 °C. ^{1}H NMR (DMSO-d_6, 400 Hz): δ 6.97 (d, J = 8.0 Hz, 2H), 7.04–7.09 (m, 6H), 7.16 (t, J = 16.0 Hz, 1H), 7.24 (d, J = 16.0 Hz, 1H), 7.31–7.36 (m, 6H), 7.52–7.58 (m, 3H), 7.65 (d, J = 8.0 Hz, 2H), 8.33 (d, J = 8.0 Hz, 1H), 8.71 (d, J = 4.0 Hz, 1H), 8.78 (s, 1H), 9.07 (s, 1H). ^{13}C NMR (100 MHz, DMSO-d_6, TMS): δ 157.8, 151.9, 150.4, 149.7, 146.9, 146.7, 135.8, 134.9, 131.6, 131.3, 129.6, 127.8, 127.6, 127.1, 126.2, 124.1, 123.3, 122.9, 121.7, 121.0. IR ν: 3029, 1591, 1509, 1488, 1330,1289, 965, 841, 759, 704, 552 cm^{-1}. MALDI-TOF m/z: calcd for [M + H]$^+$, 452.205; found, 452.990.

Preparation of 4. Compound **4** was prepared according to a procedure similar to that for **1**, using 4-pyridinecarboxaldehyde (1 g, 9.35 mmol) instead of benzaldehyde, to produce 2.5 g of orange needle crystals. Yield: 72.5%. Mp: 180 °C. ^{1}H NMR (DMSO-d_6, 400 Hz): δ 6.97 (d, J = 8.0 Hz, 2H), 7.03–7.09 (m, 6H), 7.16 (d, J = 16.0 Hz, 1H), 7.25 (d, J = 16.0 Hz, 1H), 7.33 (t, J = 8.0 Hz, 4H), 7.38 (d, J = 8.0 Hz, 2H), 7.53 (d, J = 8.0 Hz, 2H), 7.66 (d, J = 8.0 Hz, 2H), 7.86 (d, J = 8.0 Hz, 2H), 8.76 (s, 3H). ^{13}C NMR (100 MHz, DMSO-d_6, TMS): δ 158.4, 150.5, 149.1, 146.9, 146.8, 142.5, 136.4, 131.2, 129.6, 128.1, 127.6, 127.2, 126.1, 124.2, 123.3, 122. 9, 122.1, 121.9. IR ν: 3029, 1591, 1515, 1495, 1330,1288, 966, 843, 765, 697, 559 cm^{-1}. MALDI-TOF m/z: calcd for [M + H]$^+$, 452.205; found, 451.957.

Preparation of 5. Compound **5** was prepared according to a procedure similar to that for **1**, using salicylaldehyde (1.2 g, 9.83 mmol) instead of benzaldehyde, to give 2.0 g of orange-yellow powder. Yield: 58.8%. Mp: 166 °C. ^{1}H NMR (DMSO-d_6, 400 Hz): δ 6.97 (d, J = 8.0 Hz, 4H), 7.04–7.10 (m, 6H), 7.17 (d, J = 16.0 Hz, 1H), 7.26 (d, J = 16.0 Hz, 1H), 7.33 (t, J = 8.0 Hz, 4H), 7.40–7.46 (m, 3H), 7.53 (d, J = 8.0 Hz, 2H), 7.67 (d, J = 8.0 Hz, 3H), 9.03 (s, 1H), 13.18 (s, 1H). ^{13}C NMR (100 MHz, DMSO-d_6, TMS): δ 147.9, 147.6, 137.0, 133.5, 132.8, 131.6, 129.9, 129.7, 128.7, 127.8, 127.6, 126.3, 125.0, 124.1, 123.7, 123.6, 122.8, 122.0, 121.4, 119.5, 117.4. IR ν: 3027, 2922, 1617, 1590, 1508, 1490, 1329,1279, 1173, 964, 836, 754, 697, 538 cm^{-1}. HRMS (ESI-MS) m/z: calcd for [M]$^+$, 466.205; found, 466.670.

Preparation of 6. Compound **6** was prepared according to a procedure similar to that for **1**, using 4-diethylaminobenzaldehyde (1.7 g, 9.60 mmol) instead of benzaldehyde, to produce 2.7 g of yellow powder. Yield: 71.1%. Mp: 149 °C. ^{1}H NMR (DMSO-d_6, 400 Hz): δ 1.13 (s, 6H), 3.42 (m, 4H), 6.75 (d, J = 8.0 Hz, 2H), 6.97 (d, J = 8.0 Hz, 2H), 7.04–7.09 (m, 6H), 7.14–7.15 (m, 2H), 7.20 (d, J = 8.0 Hz, 2H), 7.31–7.35 (m, 4H), 7.52 (d, J = 12.0 Hz, 2H), 7.58 (d, J = 12.0 Hz, 2H), 7.72 (d, J = 8.0 Hz, 2H), 8.43 (s, 1H). ^{13}C NMR (100 MHz, DMSO-d_6, TMS): δ 160.5, 159.6, 150.1, 148.0, 147.6, 132.2, 131.1, 130.3, 129.7, 127.6, 127.4, 127.3, 127.0, 124.9, 123.9, 123.4, 121.7, 111.5, 111.4, 44.9, 12.7. IR ν: 3024, 2972, 2929, 1586, 1524, 1509, 1491, 1431, 1356, 1272, 1177, 1152, 1076, 964, 827, 753, 697, 547 cm^{-1}. HRMS (ESI-MS) m/z: calcd for [M]$^+$, 522.283; found, 522.214.

Preparation of 7. Compound **7** was prepared according to a procedure similar to that for **1**, using 4-(diethylamino)salicylaldehyde (1.9 g, 9.84 mmol) instead of benzaldehyde, to produce 2.5 g of brown powder. Yield: 63.8%. Mp: 169 °C. ^{1}H NMR (DMSO-d_6, 400 Hz): δ 1.12 (t, J = 6.0 Hz, 6H), 3.39 (m, 4H), 6.07 (s, J = 8.0 Hz, 1H), 6.33 (d, J = 8.0 Hz, 1H), 6.93–7.00 (m, 4H), 7.03–7.09 (m, 4H), 7.15–7.22 (m, 2H), 7.24–7.28 (m, 2H), 7.31–7.34 (m, 6H), 7.52 (d, J = 8.0 Hz, 2H), 7.61 (d, J = 12.0 Hz, 2H), 8.74 (s, 1H), 12.67 (s, 1H). ^{13}C NMR (100 MHz, DMSO-d_6, TMS): δ 160.5, 147.9, 147.7, 135.5, 134.2, 132.3, 132.0, 129.7, 127.8, 127.6, 126.7, 124.9, 124.2, 124.0, 123.8, 123.5, 121.5, 104.3, 97.8, 45.0. 12.9. IR ν: 3023, 2973, 2930, 1584, 1519, 1490, 1425, 1354, 1280, 1128, 965, 829, 754, 697, 545 cm^{-1}. HRMS (ESI-MS) m/z: calcd for [M + H]$^+$, 538.278; found, 538.008.

Preparation of 8. Compound **8** was prepared according to a procedure similar to that for **1**, using p-anisaldehyde (1.3 g, 9.56 mmol) instead of benzaldehyde, to produce 1.5 g of yellow powder. Yield: 42.7%. Mp: 183 °C. ^{1}H NMR (DMSO-d_6, 400 Hz): δ 3.84 (s, 3H), 6.97 (d, J = 8.0 Hz, 2H), 7.03–7.09 (m, 8H), 7.17 (d, J = 8.0 Hz, 1H), 7.26 (d, J = 8.0 Hz, 3H), 7.33 (t, J = 6.0 Hz, 4H), 7.52 (d, J = 8.0 Hz, 2H), 7.61 (d, J = 4.0 Hz, 2H), 7.90 (d, J = 8.0 Hz, 2H), 8.59 (s, 1H). ^{13}C NMR (100 MHz, DMSO-d_6, TMS): δ 162.2, 159.2, 147.9, 145.5, 139.3, 136.8, 132.1, 130.7, 129.7, 129.6, 127.8, 127.4, 124.7, 124.5, 123.6, 122.7, 121.7, 121.1, 114.5, 55.7. IR ν: 3426, 2922, 1589, 1509, 1492, 1277, 1170, 963, 837, 753, 695, 551 cm^{-1}. HRMS (ESI-MS) m/z: calcd for [M]$^+$, 480.220; found, 480.227.

Preparation of Nanoaggregates. Stock THF solutions of the compounds with a concentration of 10^{-3} mol L^{-1} were prepared. Aliquots of the stock solution were transferred to 10 mL volumetric flasks. After appropriate amounts of THF were added, water was added dropwise under vigorous stirring to furnish 5×10^{-6} mol L^{-1} solutions with different water contents (0–90 vol %). The UV–vis and PL measurements of the resultant solutions were then performed immediately.

■ ASSOCIATED CONTENT

Ⓢ Supporting Information

Spectroscopic data, absorption spectra, and fluorescence spectra of **1**–**8** in five organic solvents; absorption and PL spectra of **2**, **3**, **4**, **7**, and **8** in THF/water mixtures with different water fraction (f_w); time-resolved fluorescence curves of **1**–**8**; changes in the integrals under the emission bands with different water fractions; and NMR and mass spectra for compounds **1**–**8**. This material is available free of charge via the Internet at http://pubs.acs.org.

■ AUTHOR INFORMATION

Corresponding Author

*E-mail: zhpzhp@263.net. Fax: 86-551-63861259.

Notes

The authors declare no competing financial interest.

■ ACKNOWLEDGMENTS

This work was supported by the Program for New Century Excellent Talents in University (China), the Doctoral Program Foundation of the Ministry of Education of China (20113401110004), the National Natural Science Foundation of China (21004001, 21271003, and 21271004), the Natural Science Foundation of the Education Committee of Anhui Province (KJ2012A024), the Natural Science Foundation of Anhui Province (1208085MB22), the 211 Project of Anhui University, the Ministry of Education Funded Projects Focus on Returned Overseas Scholar, and Dr Startup funds of Anhui University (33190077).

■ REFERENCES

(1) Shirota, Y. Z. *J. Mater. Chem.* **2005**, *15*, 75.

(2) Tao, S.; Li, L.; Yu, J. S.; Jiang, Y. D.; Zhou, Y. C.; Li, C. S.; Lee, S. T.; Zhang, X. H.; Kwon, O. *Chem. Mater.* **2009**, *21*, 1284.

(3) Huang, J. H.; Su, J. H.; Li, X.; Lan, M. K.; Fung, K. M.; Fan, H. H.; Cheah, K. W.; Chen, C. H.; Tian, H. *J. Mater. Chem.* **2011**, *21*, 2957.

(4) Kim, E.; Park, S. B. *Chem.—Asian. J.* **2009**, *4*, 1646.

(5) Qiang, F.; Zhang, C. L.; Zhang, Y. M.; He, W. J.; Gao, X.; Hu, P.; Guo, Z. J. *J. Am. Chem. Soc.* **2009**, *131*, 1460.

(6) Mallick, A.; Haldar, B.; Chattopadhyay, N. *J. Phys. Chem. B* **2005**, *109*, 14684.

(7) Singh, R. B.; Mahanta, S.; Guchhait, N. *Spectrochim. Acta, Part A* **2009**, *72*, 1103.

(8) Gómez-Esteban, S.; de la Cruz, P.; Aljarilla, A.; Arellano, L. M.; Langa, F. *Org. Lett.* **2011**, *13*, 5362.

(9) Osaka, I.; Takimiya, K.; McCullough, R. D. *Adv. Mater.* **2010**, *22*, 4993.

(10) Roquet, S.; Cravino, A.; Leriche, P.; Alévêque, O.; Frère, P.; Roncali, J. *J. Am. Chem. Soc.* **2006**, *128*, 3459.

(11) Chen, Q. D.; Fang, H. H.; Xu, B.; Yang, J.; Xia, H.; Chen, F. P.; Tian, W. J.; Sun, H. B. *Appl. Phys. Lett.* **2009**, *94*, No. 201113.

(12) Fang, H. H.; Chen, Q. D.; Yang, J.; Xia, H.; Ma, Y. G.; Wang, H. Y.; Sun, H. B. *Opt. Lett.* **2010**, *35*, 441.

(13) Parthenopoulos, D. A.; Rentzepis, P. M. *Science* **1989**, *245*, 843.

(14) Belfield, K. D.; Schafer, K. J. *Chem. Mater.* **2002**, *14*, 3656.

(15) Belfield, K. D.; Liu, Y.; Negres, R. A.; Fan, M.; Pan, G. L.; Hagan, D. J.; Hernandez, F. E. *Chem. Mater.* **2002**, *14*, 3663.

(16) Zhu, Y.; Champion, R. D.; Jenekhe, S. A. *Macromolecules* **2006**, *39*, 8712.

(17) Friend, R. H.; Gymer, R. W.; Holmes, A. B.; Burroughes, J. H.; Marks, R. N.; Taliani, C.; Bradley, D. D. C.; Dos Santos, D. A.; Brédas, J. L.; Lögdlund, M.; Salaneck, W. R. *Nature* **1999**, *397*, 121.

(18) Pu, K. Y.; Liu, B. *Adv. Funct. Mater.* **2009**, *19*, 277.

(19) Jenekhe, S. A.; Osaheni, J. A. *Science* **1994**, *265*, 765.

(20) Saragi, T. P. I.; Spehr, T.; Siebert, A.; Fuhrmann-Lieker, T.; Salbeck, J. *Chem. Rev.* **2007**, *107*, 1011.

(21) Luo, J. D.; Xie, Z. L.; Lam, J. W. Y.; Cheng, L. C.; Chen, H. Y.; Qiu, C. F.; Kwok, H. S.; Zhan, X. W.; Liu, Y. Q.; Zhu, D. B.; Tang, B. Z. *Chem. Commun.* **2001**, 1740.

(22) An, B. K.; Lee, D. S.; Lee, J. S.; Park, Y. S.; Song, H. S.; Park, S. Y. *J. Am. Chem. Soc.* **2004**, *126*, 10232.

(23) Hong, Y. N.; Lam, J. W. Y.; Tang, B. Z. *Chem. Soc. Rev.* **2011**, *40*, 5361.

(24) Zhang, X. Q.; Yang, Z. Y.; Chi, Z. G.; Chen, M. N.; Xu, B. J.; Wang, C. C.; Liu, S. W.; Zhang, Y.; Xu, J. R. *J. Mater. Chem.* **2010**, *20*, 292.

(25) Dong, Y. Q.; Lam, J. W. Y.; Qin, A. J.; Li, Z.; Sun, J. Z.; Sung, H. H.-Y.; Williams, I. D.; Tang, B. Z. *Chem. Commun.* **2007**, 40.

(26) Birks, J. B. *J. Phys. B: At. Mol. Phys.* **1970**, *3*, 1704.

(27) Li, Y. P.; Li, F.; Zhang, H. Y.; Xie, Z. Q.; Xie, W. J.; Xu, H.; Li, B.; Shen, F. Z.; Ye, L.; Hanif, M.; Ma, D. G.; Ma, Y. G. *Chem. Commun.* **2007**, 231.

(28) Yu, Z. P.; Duan, Y. Y.; Cheng, L. H.; Han, Z. L.; Zheng, Z.; Zhou, H. P.; Wu, J. Y.; Tian, Y. P. *J. Mater. Chem.* **2012**, *22*, 16927.

(29) Gao, B. R.; Wang, H. Y.; Hao, Y. W.; Fu, L. M.; Fang, H. H.; Jiang, Y.; Wang, L.; Chen, Q. D.; Xia, H.; Pan, L. Y.; Ma, Y. G.; Sun, H. B. *J. Phys. Chem. B* **2010**, *114*, 128.

(30) Hu, R. R.; Lager, E.; Aguilar-Aguilar, A.; Liu, J. Z.; Lam, J. W. Y.; Sung, H. H. Y.; Williams, I. D.; Zhong, Y. C.; Wong, K. S.; Peña-Cabrera, E.; Tang, B. Z. *J. Phys. Chem. C* **2009**, *113*, 15845.

(31) Qian, Y.; Cai, M. M.; Xie, L. H.; Yang, G. Q.; Wu, S. K.; Huang, W. *ChemPhysChem* **2011**, *12*, 397.

(32) Xie, Z. Q.; Yang, B.; Cheng, G.; Liu, L. L.; He, F.; Shen, F. Z.; Ma, Y. G.; Liu, S. Y. *Chem. Mater.* **2005**, *17*, 1287.

(33) Huang, K. W.; Wu, H. Z.; Shi, M.; Li, F. Y.; Yi, T.; Huang, C. H. *Chem. Commun.* **2009**, 1243.

(34) You, Y. M.; Huh, H. S.; Kim, K. S.; Lee, S. W.; Kim, D. H.; Park, S. Y. *Chem. Commun.* **2008**, 3998.

(35) Zhen, Z.; Zhou, H. P.; Xu, G. Y.; Yu, Z. P.; Yang, X. F.; Cheng, L. H.; Kong, L.; Feng, Y.; Wu, J. Y.; Tian, Y. P. *Tetrahedron* **2012**, *68*, 6569.

(36) Zhou, H. P.; Zheng, Z.; Xu, G. Y.; Yu, Z. P.; Yang, X. F.; Cheng, L. H.; Tian, X. H.; Kong, L.; Wu, J. Y.; Tian, X. H. *Dyes Pigm.* **2012**, *94*, 570.

(37) Gao, Z. Q.; Li, Z. H.; Xia, P. F.; Wong, M. S.; Cheah, K. W.; Chen, C. H. *Adv. Funct. Mater.* **2007**, *17*, 3194.

(38) Zhang, H. G.; Tao, X. T.; Chen, K. S.; Yuan, C. X.; Yan, S. N.; Jiang, M. H. *Chin. Chem. Lett.* **2011**, *22*, 647.

(39) Zhang, X. Q.; Chi, Z. G.; Xu, B. J.; Li, H. Y.; Yang, Z. Y.; Li, X. F.; Liu, S. W.; Zhang, Y.; Xu, J. R. *Dyes Pigm.* **2011**, *89*, 56.

(40) Qin, W.; Ding, D.; Liu, J. Z.; Yuan, W. Z.; Hu, Y.; Liu, B.; Tang, B. Z. *Adv. Funct. Mater.* **2012**, *22*, 771.

(41) Shen, X. Y.; Wang, Y. J.; Zhao, E. G.; Yuan, W. Z.; Liu, Y.; Lu, P.; Qin, A. J.; Ma, Y. G.; Sun, J. Z.; Tang, B. Z. *J. Phys. Chem. C* **2013**, *117*, 7334.

(42) Zhang, X. Q.; Chi, Z. G.; Xu, B. J.; Chen, C. J.; Zhou, X.; Zhang, Y.; Liu, S. W.; Xu, J. R. *J. Mater. Chem.* **2012**, *22*, 18505.

(43) Dong, S.; Li, Z.; Qin, J. *J. Phys. Chem. B* **2009**, *113*, 434.

(44) Dong, Y. Q.; Lam, J. W. Y.; Qin, A. J.; Li, Z.; Sun, J. Z.; Sung, H. H. Y.; Williams, I. D.; Tang, B. Z. *Chem. Commun.* **2009**, 40.

(45) Yang, Z. Y.; Chi, Z. G.; Yu, T.; Zhang, X. Q.; Chen, M. N.; Xu, B. J.; Liu, S. W.; Zhang, Y.; Xu, J. R. *J. Mater. Chem.* **2009**, *19*, 5541.

(46) Chen, K. H.; Yang, J. S.; Hwang, C. Y.; Fang, J. M. *Org. Lett.* **2008**, *10*, 4401.

(47) Hong, Y. N.; Lam, J. W. J.; Tang, B. Z. *Chem. Commun.* **2009**, 4332.

(48) Tang, B. Z.; Geng, Y. H.; Lam, J. W. Y.; Li, B. S. *Chem. Mater.* **1999**, *11*, 1581.

(49) Wang, F.; Bazan, G. C. *J. Am. Chem. Soc.* **2006**, *128*, 15786.

(50) Zhu, L. N.; Yang, C. L.; Qin, J. G. *Chem. Commun.* **2008**, 6303.

(51) Strickler, S. J.; Berg, R. A. *J. Chem. Phys.* **1962**, *37*, 814.

(52) Zhao, Z. J.; Chen, S. M.; Deng, C. M.; Lam, J. W. Y.; Chan, C. Y. K.; Lu, P.; Wang, Z. M.; Hu, B. B.; Chen, X. P.; Lu, P.; Kwok, H. S.; Ma, Y. G.; Qiu, H. Y.; Tang, B. Z. *J. Mater. Chem.* **2011**, *21*, 10949.

(53) Liu, Y.; Tao, X. T.; Wang, F. Z.; Shi, J. H.; Sun, J. L.; Yu, W. T.; Ren, Y.; Zou, D. C.; Jiang, M. H. *J. Phys. Chem. C* **2007**, *111*, 6544.

(54) Dong, Y. Q.; Lam, J. W. Y.; Qin, A. J.; Liu, J. Z.; Li, Z.; Tang, B. Z.; Sun, J. X.; Kwok, H. S. *Appl. Phys. Lett.* **2007**, *91*, No. 011111.

(55) Xu, J. L.; Liu, X. F.; Lv, J.; Zhu, M.; Huang, C. S.; Zhou, W. D.; Yin, X. D.; Liu, H. B.; Li, Y. L.; Ye, J. P. *Langmuir* **2008**, *24*, 8.

(56) Shen, X. Y.; Yuan, W. Z.; Liu, Y.; Zhao, Q. L.; Lu, P.; Ma, Y. G.; Williams, I. D.; Qin, A. J.; Sun, J. Z.; Tang, B. Z. *J. Phys. Chem. C* **2012**, *116*, 10541.

(57) Li, Y. X.; Chen, Z.; Cui, Y.; Xia, G. M.; Yang, X. F. *J. Phys. Chem. C* **2012**, *116*, 6401.

(58) Zheng, Z.; Yu, Z. P.; Yang, M. D.; Jin, F.; Zhang, Q.; Zhou, H. P.; Wu, J. Y.; Tian, Y. P. *J. Org. Chem.* **2013**, *78*, 3222.

(59) Ju, H. D.; Tao, X. T.; Wan, Y.; Shi, J. H.; Yang, J. X.; Xin, Q.; Zou, D. C.; Jiang, M. H. *Chem. Phys. Lett.* **2006**, *432*, 321.

(60) Zheng, Z.; Zhang, Q.; Yu, Z. P.; Yang, M. D.; Zhou, H. P.; Wu, J. Y.; Tian, Y. P. *J. Mater. Chem. C* **2013**, *1*, 822.

(61) Zhang, H. G.; Tao, X. T.; Chen, K. S.; Yuan, C. X.; Jiang, M. H. *Synth. Met.* **2011**, *161*, 354.